symmetry

MDPI

Article

Investigation of the Impact of Household Energy Storage on DSO Grid Load Symmetry and Photovoltaic Energy Utilization Efficiency

Laurynas Šriupša [1,*], Mindaugas Vaitkūnas [1,2], Artūras Baronas [1], Gytis Svinkūnas [1], Julius Dosinas [1], Saulius Gudžius [1] and Gytis Vilutis [3]

[1] Department of Electrical and Energy Systems, Kaunas University of Technology, Studentu Str. 48, LT-51367 Kaunas, Lithuania; mindaugas.vaitkunas@ktu.lt (M.V.); arturas.baronas@ktu.lt (A.B.); gytis.svinkunas@ktu.lt (G.S.); julius.dosinas@ktu.lt (J.D.); saulius.gudzius@ktu.lt (S.G.)
[2] Faculty of Informatics, Engineering and Technologies, Kauno Kolegija Higher Education Institution, Pramones Av. 20, LT-50468 Kaunas, Lithuania
[3] Department of Applied Informatics, Kaunas University of Technology, Studentu Str. 50, LT-51368 Kaunas, Lithuania
* Correspondence: laurynas.sriupsa@ktu.edu; Tel.: +370-64016124

Abstract

In this study, we investigate the impact of electric energy storage (EES) on phase line power flow symmetry and photovoltaic (PV) energy utilization in prosumer three-phase four-wire integrated household systems. The analysis is based on high-time-resolution (1 s) experimental data collected from a real household grid and subsequent simulations of energy flows using MATLAB/Simulink software. Two converter operation strategies were evaluated: the conventional symmetric mode and the asymmetric mode developed by the authors based on an adaptive power flow management algorithm. For both strategies, the impact of EES capacity on imbalance in the distribution system operator (DSO) grid was investigated. The methodology analyzes energy flows in each phase line separately, allowing for a detailed assessment of the imbalance between phase line phenomena and their impact on local energy consumption. Key performance parameters used for the efficiency evaluation include the self-consumption and self-sufficiency rates, which quantify the share of locally generated energy consumed within the household and the degree of independence from the DSO grid. The results show that combining adaptive asymmetric inverter control with appropriately sized energy storage allows for more efficient on-site utilization of PV energy, which, at the same time, improves the load symmetry of the phase lines in the DSO grid.

Keywords: power flow symmetry; PV power plant; electric energy storage; four-wire inverter; integrated household power system; self-consumption rate; self-sufficiency rate

Academic Editors: Yi Zhang and Cheng Guo

Received: 30 March 2026
Revised: 14 May 2026
Accepted: 18 May 2026
Published: 21 May 2026

1. Introduction

According to the International Energy Agency (IEA), energy production and consumption account for approximately 75% of global greenhouse gas emissions [1]. Climate change is a global challenge that requires the development of sustainable energy strategies and the implementation of new technologies for efficient energy use. Buildings account for approximately 40% of total energy consumption and about 30% of global carbon emissions [2,3]. A growing concern is the rapidly increasing electricity demand, which leads to rising carbon emissions due to the insufficiently rapid transition from fossil fuel-based

power generation to renewable energy sources. Therefore, it is essential to not only replace traditional fossil-fuel-based energy sources with less polluting renewable energy sources but also promote more efficient and rational electricity consumption to mitigate the rapid growth in demand [4].

One of the main renewable energy technologies used to generate electricity in private households is photovoltaic (PV) systems, a large number of which have been installed in three-phase prosumer households. A characteristic feature of electricity consumption in such households is the rapid variation and uneven loading of individual phase lines. As a result, these consumers introduce load imbalance to the three-phase lines of the distribution system operator (DSO) grid. Phase load imbalance is one of the main factors leading to increased losses in distribution network lines and transformers [5]. Moreover, load imbalance is related to the efficiency of utilizing locally generated renewable energy, since simultaneous bidirectional energy flows may occur in different phase lines. In such cases, electricity may be exported to the DSO grid through one phase line while being imported from the grid through another phase line at the same time. These issues and the associated electricity distribution losses have been discussed in our previous work [6].

Various methods for mitigating load imbalance in phase lines have been proposed in the literature. In [7], a method is proposed based on real-time information obtained from smart household phase loads. The approach symmetrizes phase loading by temporarily disconnecting or reconnecting certain household loads with high thermal inertia, whose short-term switching does not cause noticeable discomfort to users. However, the implementation of this method requires significant real-time information exchange between multiple smart households and a centralized control unit. Simulation results show that this approach can reduce line energy losses by about 1.095 percentage points, which is considered a significant improvement.

In [8], load imbalance in distribution grids is reduced through the reconfiguration of imbalanced radial distribution systems. The proposed methodology focuses on an efficient three-phase load flow analysis combined with grid reconfiguration. The reconfiguration process involves strategically opening sectionalizing switches and closing tie switches based on empirical formulas and bus voltage comparisons to minimize active power losses and stabilize the system's voltage profile. The algorithm utilizes detailed component modeling, including transformers, line shunt admittances, and voltage-dependent static loads. However, the method is subject to several limitations and constraints: the analysis relies on static load models, lacking the integration of dynamic modeling necessary to account for real-time, time-varying load fluctuations. The approach requires switching operations in the DSO grid, which may introduce switching disturbances and degrade power quality. In addition, the algorithm is specifically tailored for radial distribution architectures, making its application to looped or more complex grid configurations less straightforward.

A similar load-balancing strategy for phase lines is presented in [9], where phase switching is performed within individual households. The essence of the proposed method in the provided source is an autonomous, real-time load-balancing system designed to mitigate phase imbalance in a three-phase, four-wire distribution grid. This automatic load-balancing method operates in a continuous cycle that begins with real-time monitoring, where specialized sensors measure the current, voltage, and power factor of each phase. The acquired data are stored in a control module for data analysis and comparison, which identifies the most heavily loaded and freest phases. A smart switching algorithm is then activated to instantly evaluate all possible connection combinations—totaling 36 patterns—and select the one that achieves the best possible current balance. Finally, if the detected unbalance exceeds a specific threshold, the system automatically transfers consumer loads to more suitable phases through a relay module, thereby minimizing neutral current flow

and reducing losses in the neutral wire. However, although the system tracks phase imbalance in real time, it does not balance the load continuously for every minor change; instead, it triggers reconfiguration only when the detected imbalance exceeds a predefined threshold. As in the previous case, such an approach inevitably introduces switching disturbances, which affect grid quality parameters. Moreover, this method, similarly to the previously discussed approaches, does not consider scenarios involving bidirectional energy flows in prosumer households. Therefore, it remains unclear whether such methods would be applicable under these conditions.

Another method for improving three-phase imbalance in the DSO grid, based on the Particle Swarm Current Injection method, is described in [10]. This method enhances grid stability by injecting three single-phase currents to mitigate voltage unbalance factors through steady-state control. The system utilizes a Particle Swarm Optimization (PSO) algorithm to calculate the necessary injected currents required to eliminate zero- and negative-sequence components, thereby restoring symmetrical phase magnitudes and correcting phasor angles. A primary advantage of this technique is that the compensator remains energy-neutral, balancing the phases without net energy generation or dissipation. Despite these benefits, the approach is constrained by its dependency on the PSO configuration, as inadequate iteration or particle settings can prevent the algorithm from converging on a valid solution. Furthermore, although the authors indicate that the method could be beneficial for the integration of renewable energy sources, its precise performance and efficiency during large and rapid generation fluctuations remain unclear, as the algorithm's current feasibility is tied to variations occurring in the order of minutes, and its practical application as an auxiliary service remains unclear.

In recent years, the literature has increasingly focused on electrical energy storage (EES) systems operating in conjunction with renewable energy sources in residential households to mitigate fluctuations in electricity flows and improve the local utilization of renewable energy. These systems can also contribute to grid balancing. When analyzing the performance of such hybrid systems, the selection of an appropriate time resolution for energy flow analysis becomes an important factor, which is determined by the variability in renewable energy generation and rapidly changing household consumption patterns. This is particularly relevant for households with photovoltaic (PV) systems, where their power generation depends on rapid change in meteorological conditions and seasonal periodicity. For example, the work presented in [11] analyzes the influence of time resolution on simulation accuracy using 5 min, 15 min, 30 min, and 60 min intervals. The results demonstrate that higher time resolution has a significant impact on the accuracy of techno-economic assessments. For instance, using a 5 min resolution instead of a 60 min resolution resulted in a reduction of up to 184.68% in the net present value and an increase of up to 43.12% in the discounted payback period for cost-effective EES configurations.

In another study, optimal battery sizing was performed using one year of load data with a 1 min time resolution [12]. Utilizing experimental load data together with local solar generation profiles and on-site weather data, the approach models energy flows to determine the most economically optimal battery size while accounting for the degradation of both PV modules and battery units over a one-year period. One of the objectives was to maximize energy-related metrics, specifically self-consumption and self-sufficiency. To achieve this, the model assumes that batteries are charged exclusively from renewable solar energy and not from the grid. The study also emphasizes that battery storage acts as a link to the power grid, enabling more sustainable energy consumption and reducing unpredictable power fluctuations. This is beneficial for the DSO grid, as it helps minimize sudden energy flow variations and mitigate local voltage rise issues. Furthermore, the use of high-resolution (1 min) experimental load profiles combined with real local weather data

allows for a significantly more accurate assessment of system profitability and performance compared to lower-resolution data. However, the inverter considered does not perform phase load balancing in a three-phase grid.

To supply power to the phase lines according to their individual consumption levels, an inverter capable of distributing power asymmetrically among the phases is required. Control strategies for such inverters are discussed in [13]; however, a three-phase three-wire inverter is considered, which has limited capability to distribute power asymmetrically among the three phase lines according to their demand. The system performance is further constrained by the absence of energy storage, as load balancing is limited to periods of sufficient PV generation.

In [14], the sizing of photovoltaic systems and optimal energy storage capacity is investigated using neural networks. The method employs a data-driven optimization framework for PV and battery sizing in a DC microgrid, using Long Short-Term Memory networks for load forecasting. These forecasts are integrated into a MATLAB simulation that evaluates feasible component combinations via exhaustive search to maximize the net present value while ensuring a minimum self-sufficiency ratio over a 25-year lifetime. The approach incorporates realistic factors such as seasonal irradiance, temperature variations, battery degradation, and tariff structures, enabling a detailed techno-economic assessment. However, the model assumes that excess PV generation is curtailed or exported without compensation, and net metering is not considered. Moreover, the exhaustive search may become computationally demanding for larger systems, and the use of deterministic data limits the representation of stochastic generation and consumption patterns.

Several studies have also investigated optimal PV and EES sizing for residential households using consumption and PV generation data with time resolutions of 5 min, 15 min, and 60 min [15–19]. Note that higher time resolution significantly increases the amount of processed data. However, only high-resolution data allow accurate analysis of the dynamic processes of consumption and generation within a prosumer household grid.

Active power balancing in three-phase lines using EES has been investigated through simulation studies in [20,21]. In [20], the authors propose a distributed control strategy to mitigate unbalanced active power using single-phase battery storage systems in a three-phase four-wire microgrid. In this approach, single-phase battery systems within individual households act as agents that identify their respective phase connections. These agents communicate with neighboring agents to estimate the average grid power and cooperatively operate in charging or discharging modes to minimize the deviation between their phase power and the average grid power. In [21], a three-phase optimal power flow algorithm is introduced for modeling and simulating EES operation in unbalanced distribution grids. The algorithm enables the optimization of battery operation while maintaining grid constraints, including limits on voltage unbalance in accordance with regulatory requirements. As an application scenario, this study considers the use of EES to increase the self-consumption parameter. However, although both studies are based on real input data, their time resolution is relatively low: 1 h in [20] and 15 min in [21]. Such resolutions are insufficient for accurately capturing rapid variations in electricity consumption and PV generation.

In the literature, the determination of optimal EES capacity is commonly associated with both sustainability and economic performance considerations [15,16,22–27]. The placement of energy storage within the network also significantly influences both the required capacity and operational efficiency. Strategically locating battery energy storage systems (BESSs) closer to consumer connections can reduce network losses and, consequently, lower the required storage capacity. Research in [28] indicates that configurations located at the prosumer level may require approximately 10–20% less capacity compared to transformer-side installations to achieve equivalent power flow management objectives.

Research in [29] emphasizes that the most effective solution is not a single centralized storage unit but the distribution of several storage systems across strategically selected nodes, thereby ensuring overall system robustness against uncertainties. Proper siting allows for compromise between conflicting objectives: reducing investment and energy purchase costs, stabilizing the grid voltage profile, and increasing the security margin. The study demonstrates that high photovoltaic penetration and low load levels in certain scenarios diminish the economic and technical benefits of any siting configuration, making robust siting even more critical under such conditions.

In this study, the influence of EES on phase power flow imbalance and on the efficiency of local PV energy utilization in a residential three-phase four-wire grid is investigated. Particular attention is given to the evaluation of power flow imbalance in phase lines and to the efficient distribution of locally generated PV energy within the household grid. The analysis considers the load of each phase line and distributes PV energy according to the phase load levels using an asymmetric inverter with an implemented adaptive power flow management control algorithm, thereby avoiding simultaneous bidirectional energy flows in different phase lines. The proposed approach enables more effective utilization of locally generated PV energy while simultaneously reducing power flow imbalance in the phase lines. In addition, the role of EES is evaluated in terms of its ability to further improve these parameters by reducing phase imbalance and increasing the share of locally consumed PV energy. The main contributions of this study are as follows:

- High-resolution (1 s) evaluation of the dynamic interaction between household consumption, PV generation, and EES;
- Investigation of an inverter control algorithm that balances power flows across phase lines and eliminates simultaneous bidirectional power flows in a three-phase four-wire household grid;
- Detailed assessment of the impact of EES capacity on PV energy utilization efficiency and phase power flow imbalance.

2. Methodology

This study aimed to investigate and analyze the impact of electric energy storage (EES) capacity on energy distribution symmetry and efficiency within a household grid when a photovoltaic (PV) inverter operates in both conventional symmetric mode and asymmetric mode. The study was based on the computer simulation of energy flows in a three-phase four-wire household grid using primary data collected during an experiment conducted in a selected household.

2.1. Collection of Primary Data

Primary data were obtained using a measurement system composed of two smart three-phase electricity meters, M1 and M2 (Figure 1), developed by the authors and deployed in a Lithuanian household with an installed power capacity of 20 kW. The household grid comprised a 10 kWp PV power plant and a symmetrically operating inverter without an EES system [30]. One bidirectional smart meter (Smart Meter M1) was used to measure both imported and exported power flows in each phase line (P_{dsoL1}, P_{dsoL2}, and P_{dsoL3}), while another bidirectional smart meter (Smart Meter M2) was used to measure the power flows at the outputs of the three-phase symmetric PV inverter (P_{invL1}, P_{invL2}, and P_{invL3}). The smart meters measured the average active power flows in real time using a predefined time resolution Δt, and transmitted these data to a remote SQL server for storage. The measuring accuracy of the smart meters was 1%, and the maximum time resolution was 1 s. Measurements were carried out from April to October 2023.

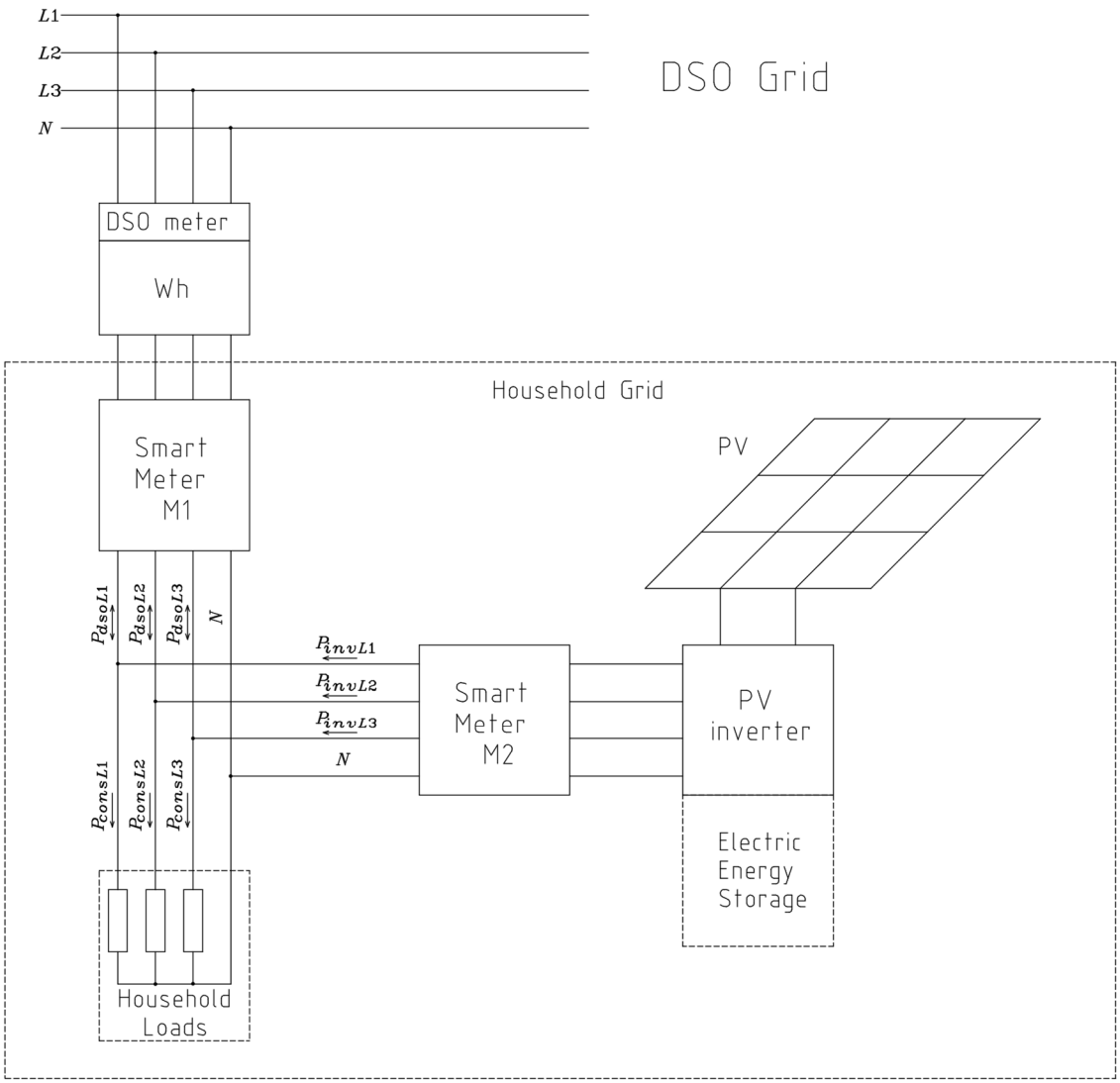

Figure 1. Household energy flow measurement system.

In the case of the asymmetric mode inverter, the inverter's output data P'_{invL1}, P'_{invL2}, and P'_{invL3} were simulated using the MATLAB (version R2023b) Simulink software and the real measured data of the symmetric inverter, P_{invL1}, P_{invL2}, and P_{invL3}. The remaining household power flows for each time interval Δt were determined as follows: the load (consumption) power flows of each of the three phase lines L_i (i = 1, 2, 3):

$$P_{consLi} = P_{invLi} - P_{dsoLi}; \quad (1)$$

the total load power:

$$P_{cons} = P_{consL1} + P_{consL2} + P_{consL3} = \sum_{i=1}^{3} P_{consLi}; \quad (2)$$

the power generated by the PV power plant:

$$P_{pv} = P_{invL1} + P_{invL2} + P_{invL3} = \sum_{i=1}^{3} P_{invLi} = P_{inv}. \quad (3)$$

Here, the total PV power P_{pv}, generated during the time interval Δt, was assumed to be equal to the total inverter output power P_{Tinv}, since inverter power losses were considered negligible and therefore not taken into account.

The energy generated by the PV power plant E_{PV} and the energy consumed in the household E_{CONS} over the investigated period (one day in our case) were calculated by integrating (summing) the corresponding powers over all j-th time intervals Δt:

$$E_{PV} = \Delta t \sum_{j=1}^{N} P_{pv\ j} = \Delta t \cdot P_{PV}, \quad (4)$$

$$E_{CONS} = \Delta t \sum_{j=1}^{N} P_{cons\ j} = \Delta t \cdot P_{CONS}, \quad (5)$$

where N is the number of Δt time intervals; P_{PV}, generated PV power; and P_{CONS}, power consumed over the investigated period.

As mentioned above, the initially measured and calculated household data were used as primary input data for the household grid simulation and analysis. Based on these data, the household grid power flows were analyzed through the simulation of inverter operation with an EES system of variable capacity under both symmetric and asymmetric operating modes. The asymmetric mode was simulated using the adaptive power flow management (APFM) algorithm proposed by the authors [30]. The adaptivity of the APFM algorithm is achieved by controlling the inverter output power according to the load levels in each of the three-phase grid lines. During the simulations, the storage energy capacity (EC) was varied from zero (no EES connected or utilized) to the maximum value EC_{max}, in increments of ΔEC.

2.2. Electrical Energy Storage Control Algorithm

The household EES control algorithm developed by the authors is intended for the adaptive control of EES charging and discharging under various household grid operating conditions, taking into account the instantaneous power generated by the PV system P_{pv} and the power consumed by household users P_{cons}. For this purpose, an ideal EES model was selected, which does not consider any chemical or electrochemical processes occurring inside the storage device. Such an EES model allows for simpler simulation of the electrical processes required to evaluate mutual energy exchange among the PV system, inverter, EES, and power grid.

The EES is characterized by the following properties and assumptions:

- The EES is charged with PV energy only;
- The internal resistance is assumed to be zero, and the storage can conduct unlimited charging or discharging current during the energy exchange;
- The storage EC is assumed to be constant throughout the energy exchange process and can be set differently for each simulation case;
- The EES has no losses or self-discharge;
- All stored energy can be extracted from the EES by discharging it down to a zero state of charge;
- The energy remaining in the EES for the next day is not considered.

Figure 2 presents one cycle of the EES control algorithm, which performs the sequence of operations shown in the figure using input (primary) data obtained during a single time interval Δt.

The entire EES charging and discharging control process consists of a continuous sequence of control algorithm cycles. At the beginning of the operation of the control algorithm, the capacity of the ideal EES and the time resolution interval of the input data Δt are defined. These parameters remain constant throughout all algorithm operations. In the next step, data on the EES initial energy level EL are provided, as well as the average generated and consumed powers P_{pv} and P_{cons} during time interval Δt. These data change at each Δt interval.

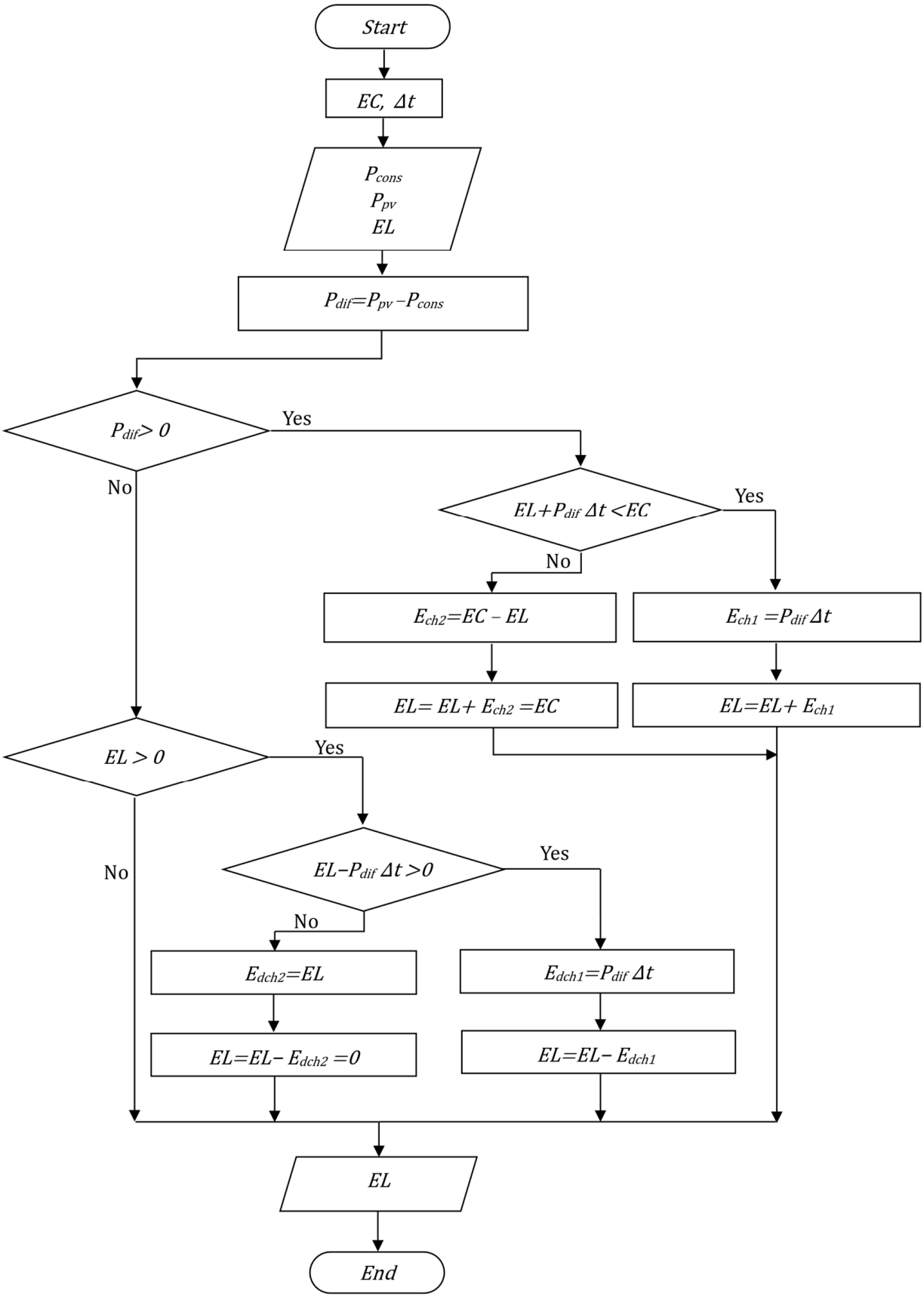

Figure 2. EES charging and discharging control algorithm.

First, the algorithm evaluates the power imbalance between P_{pv} and P_{cons}; that is, it calculates the difference between the generated and consumed power:

$$P_{dif} = P_{pv} - P_{cons}. \tag{6}$$

Depending on the sign of this power imbalance P_{dif}, the storage is charged or discharged accordingly.

If the PV system generates more power than the household consumes, the power imbalance P_{dif} is positive ($P_{dif} > 0$), and whether the storage is not yet fully charged and can still accept an amount of energy E_{ch1} is then checked:

$$E_{ch1} = P_{dif} \cdot \Delta t. \tag{7}$$

The verification condition is expressed as

$$EL + P_{dif} \cdot \Delta t < EC \tag{8}$$

If this condition is satisfied, the storage EL is increased by the amount of energy E_{ch1}:

$$EL = EL + E_{ch1}. \tag{9}$$

If condition (8) is not satisfied, only the amount of energy required to reach full charge E_{ch2} is directed to the storage:

$$E_{ch2} = EC - EL. \tag{10}$$

The EES then becomes fully charged, i.e.,

$$EL = EL + E_{ch2} = EC. \tag{11}$$

When the PV system generates less (or equal) power than the household consumes ($P_{dif} \leq 0$), the EES energy is used to cover consumption. In this case, the algorithm checks whether the storage is not fully discharged (condition $EL > 0$) and, if this condition is satisfied, verifies whether the stored energy is sufficient to cover the current energy consumption:

$$EL - P_{dif} \cdot \Delta t > 0. \tag{12}$$

If the stored energy is sufficient, it is used to cover consumption. Then, the storage energy amount is reduced by

$$E_{dch1} = P_{dif} \cdot \Delta t, \tag{13}$$

and the EES energy acquires a new value

$$EL = EL - E_{dch1}. \tag{14}$$

If the stored energy is insufficient, all remaining energy is taken from the storage for consumption:

$$E_{dch2} = EL. \tag{15}$$

The storage is then fully discharged, and its EL becomes

$$EL = EL - E_{dch2} = 0. \tag{16}$$

The process based on this algorithm is repeated in the next cycle, using the newly obtained storage EL and the P_{pv} and P_{cons} data values of the subsequent Δt interval.

3. Simulation of Power Flows in a Household Grid

The power flows between the PV system, EES, and inverter were simulated using the previously described EES charging and discharging control algorithm and data obtained experimentally from a real household. Both the symmetric and asymmetric inverters operating according to the APFM algorithm were simulated and analyzed separately.

In the absence of an EES system, the entire PV power P_{pv} is transferred to the inverter, and the total (summed over all phase lines) output power of the symmetric inverter P_{Tinv}, and output power of the asymmetric inverter P'_{Tinv} are equal:

$$P_{Tinv} = P'_{Tinv} = P_{pv}. \tag{17}$$

As previously noted, when simulating an inverter with an ideal EES system, energy losses in both the energy storage and inverter were not considered. Energy generated by the PV system that exceeds the total household consumption is stored in the EES. Thus, the EES charging process occurs when the power difference between the PV generation P_{pv} and household consumption P_{cons} is positive. In this case, the storage is charged either with the full surplus energy or only up to its maximum capacity EC, in case the available surplus energy together with the energy already stored would exceed the maximum capacity:

$$E_{ch} = \begin{cases} E_{ch1} = P_{dif} \cdot \Delta t, & if \;\; EL + P_{dif} \cdot \Delta t < EC, \\ E_{ch2} = EC - EL, & if \;\; EL + P_{dif} \cdot \Delta t \geq EC. \end{cases} \tag{18}$$

Accordingly, the total power delivered by both the symmetric inverter (P_{Tinv}) and asymmetric inverter (P'_{Tinv}) to the household grid is reduced as follows:

$$P_{Tinv} = P'_{Tinv} = P_{pv} - \frac{E_{ch}}{\Delta t} \tag{19}$$

If the total inverter power P_{Tinv} or P'_{Tinv} exceeds the total household consumption power P_{cons}, for example, when the storage is fully charged ($EL = EC$), the surplus power is exported to the DSO grid.

If the PV generation power is lower than the total household consumption ($P_{dif} \leq 0$) and energy is available in the storage ($EL > 0$), the lacking energy is supplied to the inverter from the storage. Consequently, the storage is discharged depending on the amount of stored energy EL. The discharged energy is defined as

$$E_{dch} = \begin{cases} E_{dch1} = P_{dif} \cdot \Delta t, & if \;\; EL - P_{dif} \cdot \Delta t > 0\,, \\ E_{dch2} = EL, & if \;\; EL - P_{dif} \cdot \Delta t \leq 0\,. \end{cases} \tag{20}$$

In this case, the total inverter output power is increased to

$$P_{Tinv} = P_{pv} + \frac{E_{dch}}{\Delta t}, \tag{21}$$

If the energy in storage is insufficient or unavailable ($EL = 0$), the inverter supplies only part of the household power demand, and the remaining required power is imported from the DSO grid.

However, the distribution of inverter output power among the phase lines differs depending on the inverter operating mode. For an inverter operating in symmetric mode, the output powers are equal across all phase lines:

$$P_{invL1} = P_{invL2} = P_{invL3} = \frac{1}{3P_{Tinv}}. \tag{22}$$

In the case of an adaptive inverter operating in asymmetric mode based on the APFM algorithm proposed in [30], the output power is distributed across the phase lines according to their respective loads and is typically unequal. The load power values can subsequently be evaluated as follows: first, the load power values of all three phases are sorted in ascending order, and the power imbalances Δ1 and Δ2 are determined:

$$\begin{aligned} \Delta 1 &= P_{consLmax} - P_{consLmed}, \\ \Delta 2 &= P_{consLmed} - P_{consLmin}, \end{aligned} \tag{23}$$

where $P_{consLmax} = max(P_{consLi})$, $P_{consLmed} = med(P_{consLi})$, and $P_{consLmin} = min(P_{consLi})$.

If the photovoltaic system generates a low power level, i.e., $P_{Tinv} \leq \Delta 1$, all of the generated power of the asymmetric inverter is directed to the most heavily loaded phase line. In this case, the output powers of the three-phase inverter are as follows:

$$\begin{aligned} P'_{invLmax} &= P_{Tinv}, \\ P'_{invLmed} &= 0, \\ P'_{invLmin} &= 0. \end{aligned} \tag{24}$$

Here $P'_{invL\max}$, $P'_{invL\mathrm{med}}$, and $P'_{invL\min}$ denote the inverter output powers corresponding to the most heavily, moderately, and least loaded phase lines, respectively.

If the PV system generates a higher power level, i.e., $\Delta 1 < P_{Tinv} \leq \Delta 1 + 2{\cdot}\Delta 2$, the inverter output power is allocated between the two most heavily loaded phase lines:

$$\begin{aligned} P'_{invLmax} &= \Delta 1 + (P_{Tinv} - \Delta 1)/2, \\ P'_{invLmed} &= (P_{inv} - \Delta 1)/2, \\ P'_{invLmin} &= 0. \end{aligned} \tag{25}$$

When the PV system generates a high-power level, i.e., $P_{Tinv} > \Delta 1 + 2{\cdot}\Delta 2$, the inverter output power is allocated across all three phase lines:

$$\begin{aligned} P'_{invLmax} &= \Delta 1 + \Delta 2 + (P_{inv} - \Delta 1 - 2{\cdot}\Delta 2)/3, \\ P'_{invLmed} &= \Delta 2 + (P_{inv} - \Delta 1 - 2{\cdot}\Delta 2)/3, \\ P'_{invLmin} &= (P_{inv} - \Delta 1 - 2{\cdot}\Delta 2)/3. \end{aligned} \tag{26}$$

The total output power of the asymmetric inverter is

$$P'_{Tinv} = P'_{invL\max} + P'_{invL\mathrm{med}} + P'_{invL\min} = \sum_i P'_{invLi}, \tag{27}$$

where $i = 1, 2, 3$.

After determining the inverter phase line power flows P_{invLi} and P'_{invLi} for each Δt interval, and using the measured household load power flows P_{consLi}, the power flows between the household and DSO grid (P_{dsoLi}, P'_{dsoLi}), as well as the import (P_{impLi}, P'_{impLi}) and export (P_{expLi}, P'_{expLi}) power flows, are calculated for both inverter operating modes. For the symmetric inverter operating mode,

$$P_{dsoLi} = P_{invLi} - P_{consLi}, \tag{28}$$

$$P_{impLi} = \begin{cases} |P_{dsoLi}|, & if \;\; P_{dsoLi} < 0 \\ 0, & otherwise. \end{cases}, \tag{29}$$

$$P_{expLi} = \begin{cases} |P_{dsoLi}|, & if \;\; P_{dsoLi} > 0 \\ 0, & otherwise. \end{cases}. \tag{30}$$

Analogously, these flows are determined for the inverter operating in adaptive asymmetric mode:

$$P'_{dsoLi} = P'_{invLi} - P_{consLi}, \tag{31}$$

$$P'_{impLi} = \begin{cases} |P'_{dsoLi}|, & if \;\; P'_{dsoLi} < 0 \\ 0, & otherwise. \end{cases}, \tag{32}$$

$$P'_{expLi} = \begin{cases} |P'_{dsoLi}|, & if \;\; P'_{dsoLi} > 0 \\ 0, & otherwise. \end{cases}. \tag{33}$$

The total import P_{imp} and export P_{exp} powers summed over all three phase lines for the symmetric inverter are calculated as

$$P_{imp} = \sum_i P_{impLi}, \tag{34}$$

$$P_{exp} = \sum_i P_{expLi}, \tag{35}$$

and analogously for the asymmetric inverter,

$$P'_{imp} = \sum_i P'_{impLi}, \tag{36}$$

$$P'_{exp} = \sum_i P'_{expLi}. \tag{37}$$

Power imbalances P_{imb} and P'_{imb} in the DSO grid caused by household phase line loads in both cases were evaluated as the difference between the maximum and minimum of phase line powers:

$$P_{imb} = \max_{i=1,2,3} P_{dsoLi} - \min_{i=1,2,3} P_{dsoLi}, \tag{38}$$

$$P'_{imb} = \max_{i=1,2,3} P'_{dsoLi} - \min_{i=1,2,3} P'_{dsoLi}. \tag{39}$$

From the obtained data, the daily imported energy deficit E_{IMP} and surplus exported energy E_{EXP} were calculated for the symmetric inverter operating mode as

$$E_{IMP} = \Delta t \sum_{j=1}^{N} P_{imp\ j} = \Delta t \cdot P_{IMP}, \tag{40}$$

$$E_{EXP} = \Delta t \sum_{j=1}^{N} P_{exp\ j} = \Delta t \cdot P_{EXP}, \tag{41}$$

and for the adaptive asymmetric inverter operating mode as

$$E'_{IMP} = \Delta t \sum_{j=1}^{N} P'_{imp\ j} = \Delta t \cdot P'_{IMP}, \tag{42}$$

$$E'_{EXP} = \Delta t \sum_{j=1}^{N} P'_{\exp\ j} = \Delta t \cdot P'_{EXP}. \tag{43}$$

Here, P_{IMP}, P_{EXP}, P'_{IMP}, and P'_{EXP} are the daily values of the import and export powers of inverters operating in symmetric and asymmetric modes, respectively.

Similarly, the daily imbalance energy was found for the inverter's symmetrical and asymmetrical operating modes:

$$E_{IMB} = \Delta t \sum_{j=1}^{N} P_{imbj}, \tag{44}$$

$$E'_{IMB} = \Delta t \sum_{j=1}^{N} P'_{imbj}. \tag{45}$$

The influence of storage capacity EC on energy distribution and consumption efficiency in the household grid was evaluated using two parameters. The self-sufficiency rate (SSR) represents the percentage of energy consumed in the household that originates from

local generation relative to the total energy consumption during the investigated period. The self-consumption rate (SCR) represents the percentage of locally generated energy that is consumed locally relative to the total energy generated by that source during the investigated period. For the inverter operating in symmetric mode,

$$SSR = \frac{E_{CONS} - E_{IMP}}{E_{CONS}} \cdot 100\% = \frac{\sum_{j=1}^{N} (P_{cons\ j} - P_{imp\ j})}{\sum_{j=1}^{N} P_{cons\ j}} \cdot 100\%, \quad (46)$$

$$SCR = \frac{E_{PV} - E_{EXP}}{E_{PV}} \cdot 100\% = \frac{\sum_{j=1}^{N} (P_{pv\ j} - P_{exp\ j})}{\sum_{j=1}^{N} P_{pv\ j}} \cdot 100\%. \quad (47)$$

For the inverter operating in adaptive asymmetric mode, these indicators are defined as

$$SSR' = \frac{E_{CONS} - E'_{IMP}}{E_{CONS}} \cdot 100\% = \frac{\sum_{j=1}^{N} (P_{cons\ j} - P'_{imp\ j})}{\sum_{j=1}^{N} P_{cons\ j}} \cdot 100\%, \quad (48)$$

$$SCR = \frac{E_{PV} - E'_{EXP}}{E_{PV}} \cdot 100\% = \frac{\sum_{j=1}^{N} (P_{pv\ j} - P'_{\exp j})}{\sum_{j=1}^{N} P_{pv\ j}} \cdot 100\%. \quad (49)$$

4. Simulation Results

A simulation-based analysis was conducted to evaluate the influence of EES capacity on phase line power flow asymmetry and the efficiency of the PV energy distribution between the household and DSO grid. All calculations were performed with a time resolution of $\Delta t = 1$, resulting in $N = 86,400$ samples per day for each parameter. For each day, a series of simulations was carried out by uniformly varying the storage capacity from $EC_0 = 0$ Wh to $EC_{max} = 8$ kWh with a step of $\Delta EC = 50$ Wh. Thus, 160 grid operating scenarios associated with different storage capacities were generated and examined.

The analysis encompassed eleven representative days selected from a seven-month measurement period. Table 1 presents the generated and consumed energies in a household without an EES for each of those eleven days: the daily generated energy E_{PV}, found according to (4); the energy consumed in separate phase lines $E_{CONS\ L1}$, $E_{CONS\ L2}$, and $E_{CONS\ L3}$ (1) and in total E_{CONS} during the day (5). Although these energies were obtained under symmetric inverter operation, their values are independent of the inverter type.

Table 1. Comparison of household energy generation, consumption, and imbalance over eleven selected days.

Day	E_{PV}, kWh	$E_{CONS\ L1}$, kWh	$E_{CONS\ L2}$, kWh	$E_{CONS\ L3}$, kWh	E_{CONS}, kWh	E_{IMB} kWh
9 April 2023	43.8	3.6	17.2	4.6	25.3	15.3
15 April 2023	23.1	4.1	17.2	5.1	26.4	14.2
20 April 2023	69.1	2.6	18.0	5.8	26.3	17.0
5 May 2023	80.4	5.1	13.7	4.7	23.5	9.6
12 May 2023	81.0	2.1	13.8	2.5	18.4	13.3
27 May 2023	83.3	0.8	12.1	0.8	13.7	12.0
6 June 2023	87.3	2.1	12.0	2.3	16.5	14.4
18 June 2023	30.4	0.6	13.4	2.3	16.4	14.6
24 June 2023	63.2	0.4	5.9	0.2	6.5	5.7
1 July 2023	60.1	2.2	10.4	0.6	13.3	11.5
23 September 2023	41.0	4.7	7.7	2.3	14.7	11.6

Uneven loading of the household grid phase lines was observed on all days. The last column of the table presents the calculated values of the total imbalance energy in phase lines for symmetric inverter mode E_{IMB} (44). The unequal loading of household grid phase lines results in power imbalance, negatively impacting the DSO grid. Thus, power imbalance represents a significant performance indicator of the household electrical system.

4.1. Impact of Primary Data Time Resolution on Simulation Results

The accuracy of power flow evaluation depends on the time resolution of the input data. Conventional household electricity meters used for DSO billing generally provide data with a one-hour time resolution, whereas newer smart DSO meters provide data aggregated over 15-min intervals. Many studies reported in the literature were conducted using data with such time resolutions. Higher time resolution allows for a more precise evaluation of the influence of short-term rapidly changing fluctuations in generation and consumption on grid qualitative parameters. However, it simultaneously leads to a substantial increase in data volume and computational complexity. To evaluate the impact of one-second resolution on the accuracy of simulation results, simulations using 1 s, 15 min, and 1 h time resolutions were compared. The instantaneous power imbalance P_{imb} in the phase lines was chosen as the evaluation parameter because it is directly related to consumption and can change rapidly over time. The investigation was carried out without considering the presence of an energy storage system.

In the symmetric inverter mode, the initial one-second import and export power data of each phase line P_{dsoLi} (where i = 1, 2, 3), acquired from smart meter M1 (Figure 1), were resampled to the required time resolutions. The values for each phase over the analyzed period were recalculated according to the following rule, while generating a new time-series dataset:

$$\left\{ \sum_{j=1}^{M} P_{dsoLi\ j}; \sum_{j=M+1}^{2M} P_{dsoLi\ j}; \sum_{j=2M+1}^{3M} P_{dsoLi\ j}; \ldots \sum_{j=(n-1)M+1}^{N} P_{dsoLi\ j} \right\} = \{P_{dsoLi\ 1}; P_{dsoLi\ 2}; P_{dsoLi\ 3}; \ldots P_{dsoLi\ n}\}. \quad (50)$$

Here, i = 1, 2, 3; M denotes the number of one-second power samples aggregated to form each new sample; N, as defined previously, is the total number of one-second power samples over the investigated period; and $n = \frac{N}{M}$ represents the number of samples at the new time resolution within the analyzed period.

For a 15 min time resolution (Δt = 15 min = 900 s), M = 9000; for a 1 h resolution Δt = 1 h = 3600 s), M = 3600. Since the investigated period corresponds to one day (86,400 s), $N = 86,400$. Consequently, the number of new time samples per day is $n = 96$ in the first case and $n = 24$ in the second.

Having obtained the P_{dsoLi} datasets corresponding to different time resolutions and the respective number of samples n, the imbalance values P_{imb} for all analyzed days were calculated using expression (38).

For visualization purposes, Figure 3 presents the resulting P_{imb} values for 15 April (a), characterized by relatively low PV generation, and 6 June (b), when PV generation is significantly higher. The green curves correspond to a 1 s resolution, the red curves to 15 min, and the blue curves to 1 h. As evident from these examples, neither the 15 min nor, especially, the 1 h resolution is sufficient to capture short-term imbalance peaks, which may be up to an order of magnitude higher than those observable at coarser resolutions. Under such conditions, short-duration power imbalances cannot be accurately assessed or effectively compensated.

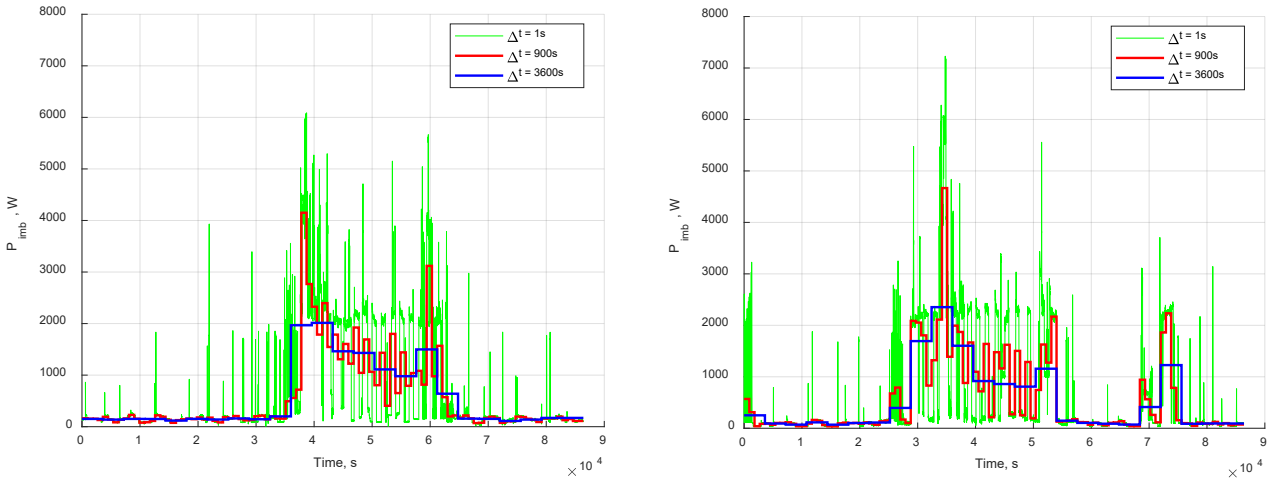

(**a**) (**b**)

Figure 3. Dependence of imbalance P_{imb} on primary data time resolution for 15 April (**a**) and 6 June (**b**).

Table 2 presents the imbalance parameters for all investigated days calculated from the measurement results with a time resolution of 1 s, as well as the values simulated from the same measurements assuming time resolutions of 15 min and 1 h (50). The table includes the daily mean imbalance $\overline{P}_{imb}$; the standard deviation σ, indicating how dispersed the data are relative to the mean; and the maximum daily imbalance $\max_j P_{imbj}$ (where j = 1, 2, . . ., n, and n is the number of samples per day). The bottom row of the table presents the averages of these parameters across all investigated days.

Table 2. Three-phase line imbalance parameters at three different time resolutions.

Day	$\overline{P}_{imb}$			σ,W			$\max_j P_{imbj}$,W		
	Δt = 1 s	**Δt = 900 s**	**Δt = 3600 s**	**Δt = 1 s**	**Δt = 900 s**	**Δt = 3600 s**	**Δt = 1 s**	**Δt = 900 s**	**Δt = 3600 s**
9 April 2023	624.7	613.7	602.8	899.4	707.7	573.3	5759.3	3529.5	2060.7
15 April 2023	592.9	574.1	579.6	933.5	770.0	645.1	6087.6	4150.2	2013.7
20 April 2023	701.3	678.9	674.4	964.8	794.1	710.6	5819.6	3429.9	2416.4
5 May 2023	376.8	377.2	383.1	628.5	467.9	348.3	6285.6	2408.5	1190.5
12 May 2023	539.9	539.1	546.8	777.9	552.1	437.7	4513.9	2335.9	1469.9
27 May 2023	506.4	499.6	503.5	861.1	656.9	540.8	5307.7	3164.8	1949.6
6 June 2023	586.7	572.9	557.8	968.7	788.0	639.4	7228.9	4666.8	2353.4
18 June 2023	606.9	594.5	577.4	962.3	823.9	765.2	5576.9	3026.6	2703.5
24 June 2023	234.6	234.8	241.0	502.0	358.3	239.9	2954.4	2035.1	938.1
1 July 2023	470.3	464.6	471.7	810.9	611.6	494.2	4908.5	3703.2	1953.2
23 September 2023	456.4	394.4	354.9	725.0	556.4	495.6	5941.6	2957.8	2423.3
Average	517.9	504.0	499.4	821.3	644.3	535.5	5489.4	3218.9	1952.0

It can be observed that with the highest time resolution (1 s), both the average imbalance and standard deviation are generally larger than those obtained with lower resolutions (900 s and 3600 s). This indicates that lower time resolutions fail to capture short-term imbalance variations, leading to less accurate results. This effect is particularly evident

in the values of the maximum daily imbalance $\max_j P_{imbj}$. On average, the values obtained for Δt = 1 s are 1.7 times higher than those for Δt = 900 s and 2.8 times higher than those for Δt = 3600 s. For example, on 5 May, these differences increased to 2.6 and 5.3 times, respectively.

4.2. Dependence of Energy Import and Export Parameters on Storage Capacity

The following graphs present the simulated dependencies of the grid parameters on the EES capacity. Figure 4 presents the dependencies of total daily energy flows on storage capacity in the case of a symmetric inverter: Figure 4a shows the dependence of the daily energy exported to the DSO grid E_{EXP}, and Figure 4b, the corresponding dependencies of the daily imported energy E_{IMP}. The colors of the curves correspond to different days, as indicated in the legend of Figure 4a, and are consistent across all figures. As can be seen, all of these dependencies are nonlinear. In the case of energy import, the most pronounced reduction is observed at small storage capacities (up to 100–500 Wh). With further increases in storage capacity, the rate of decrease in this parameter slows down until a breakpoint capacity value is reached, beyond which the parameter typically stabilizes or may even begin to increase. The rise in import after the breakpoint is due to phase line load asymmetry and will be examined in detail later in this section.

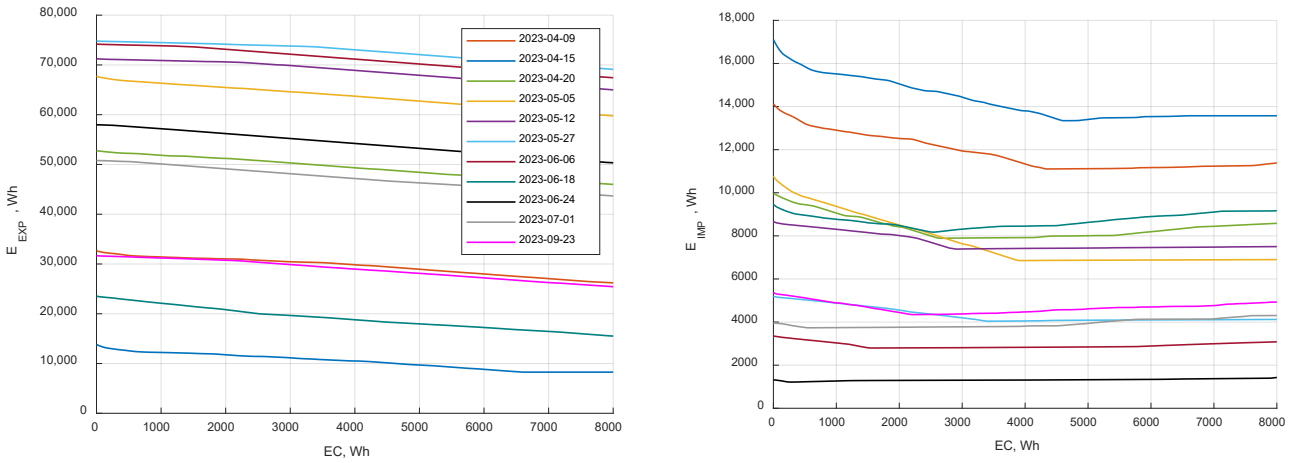

(**a**) (**b**)

Figure 4. Dependence of energy flows E_{EXP} (**a**) and E_{IMP} (**b**) on storage capacity in symmetric inverter mode simulation.

In general, the breakpoint capacity values indicate the threshold beyond which further increases in storage capacity become impractical, as they no longer improve the quality indicators of energy distribution in the grid—parameters *SCR* and *SSR*. The breakpoint capacity value differs for export and import, and as revealed by further investigations, it depends on the specific day's generation and consumption conditions. Moreover, for all days except 15 April, the export breakpoint was not reached due to insufficient storage capacity *EC*. The breakpoint is associated with the maximum amount of PV energy that can be accumulated over a day. With increasing storage capacity, the capacity level at which the entire daily PV generation is stored in the battery can always be reached, where energy export is reduced to its minimum value and remains constant thereafter. In the case of a symmetric inverter, it is not possible to reduce energy export to zero due to bidirectional energy flows, which occur in the grid phase lines.

Next, Figure 5 presents the dependence of the energy flows on storage capacity in the asymmetric inverter mode for all of the aforementioned days. As expected, lower energy export (Figure 5a) and import (Figure 5b) flows were obtained in this case.

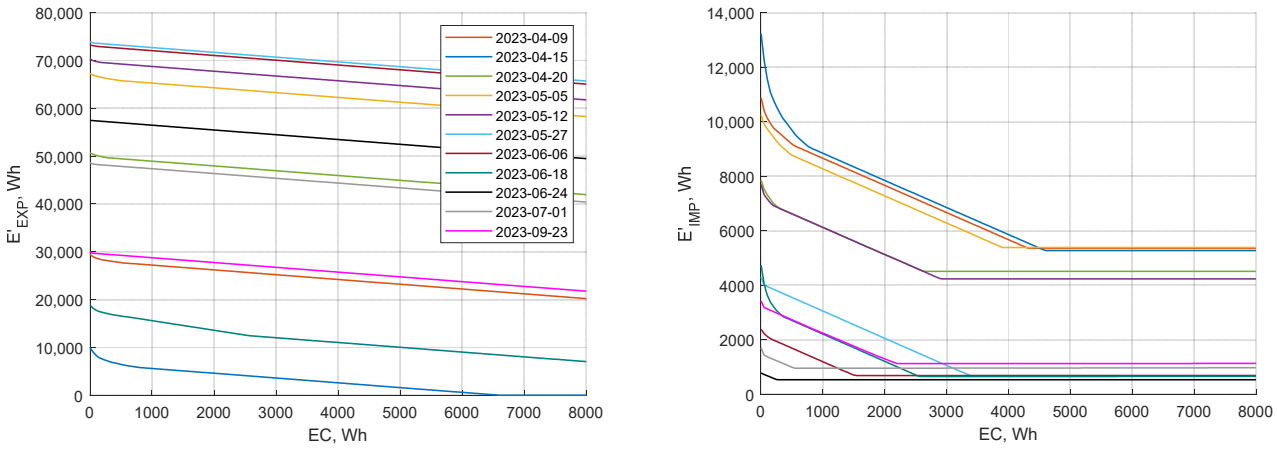

(**a**) (**b**)

Figure 5. Dependence of energy flows E'_{EXP} (**a**) and E'_{IMP} (**b**) on storage capacity in asymmetric inverter mode simulation.

Nonetheless, the breakpoint capacities for both import and export were identical to those observed for the symmetric inverter. The main difference here is that, beyond the breakpoint, the imported energy values stabilize and no longer increase. This is because, as the storage capacity increases, a threshold is reached at which the energy stored during the day is sufficient to maintain the symmetrization of import and export energy flows in the grid phase lines until the end of the day. Moreover, in the case of the asymmetric inverter, energy export can be reduced to zero if the storage capacity is sufficient, as, for example, on 15 April.

Table 3 summarizes the average energy import ($\overline{E_{IMP}}$, $\overline{E'_{IMP}}$), export ($\overline{E_{EXP}}$, $\overline{E'_{EXP}}$), and imbalance ($\overline{E_{IMB}}$, $\overline{E'_{IMB}}$) values for all analyzed days as the storage capacity varied from 0 kWh to 8 kWh in 1 kWh steps. When considering all 11 days, the EES with a capacity of 8000 Wh enabled an average reduction in energy import of 16% in the symmetric inverter mode and 56% in the asymmetric inverter mode. Meanwhile, energy export was reduced by 13% and 19%, respectively. These results clearly indicate that the asymmetric inverter power flow balancing improves EES utilization, enhancing PV energy distribution efficiency and grid performance parameters.

Table 3. Average values of energy import, export, and imbalance across 11 days for different EES capacities.

Day	***EC*, Wh**								
	0	**1000**	**2000**	**3000**	**4000**	**5000**	**6000**	**7000**	**8000**
$\overline{E_{IMP}}$, Wh	8116.3	7430.1	7076.4	6733.7	6568.4	6569.7	6663.1	6737.6	6815.6
$\overline{E'_{IMP}}$, Wh	6115.6	4383.0	3617.2	3052.1	2756.4	2674.8	2675.5	2675.7	2676.2
$\overline{E_{EXP}}$, Wh	50,100.7	49,238.3	48,568.4	47,745.6	46,878.8	45,962.6	45,056.0	44,167.1	43,336.1
$\overline{E'_{EXP}}$ Wh	48,157.8	46,243.3	45,152.5	44,102.2	43,102.6	42,103.0	41,104.3	40,141.6	39,233.1
$\overline{E_{IMB}}$, Wh	12,429.8	12,429.8	12,429.8	12,429.8	12,429.8	12,429.8	12,429.8	12,429.8	12,429.8
$\overline{E'_{IMB}}$, Wh	2678.7	1642.2	1134.5	890.4	772.4	754.3	755.6	756.0	756.9

The total daily imbalance energy $\overline{E'_{IMB}}$ in the case of the asymmetric inverter mode depends on the storage capacity, and its variation over the eleven days is shown in Figure 6. The imbalance energy initially decreases rapidly at small capacities, and then stabilizes and remains constant as the capacity increases. The imbalance energy stabilization level is determined by the simulation approach, which assumes an initially empty battery and no available PV energy during the early hours of the day.

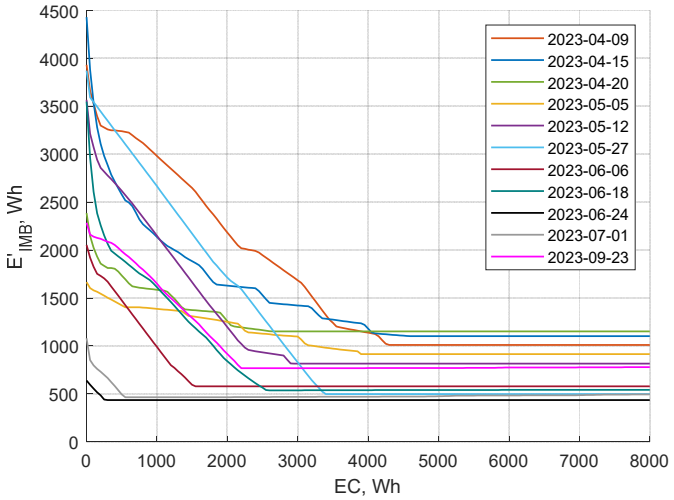

Figure 6. Dependence of the total imbalance energy E'_{IMB} on storage capacity in the asymmetric inverter mode simulation.

Only in the morning, when PV generation begins, does the inverter's APFM algorithm become active, reducing the power flow imbalance in the grid phase lines. Energy imported asymmetrically into the household grid phase lines before this generation is not influenced by the storage capacity, thereby determining the total daily energy flow imbalance. The breakpoints of imbalance energy stabilization coincide with those observed in the imported energy curves (Figure 5b).

As can be seen from Table 3, the EES with a capacity of 8000 Wh let us achieve an average reduction of 72% in daily imbalance energy under asymmetric inverter operation. However, this parameter varied considerably from day to day. The greatest reduction ranged from 32% on 24 June to 75% on 15 April. This parameter is strongly correlated with energy consumption and, consequently, with energy import: according to measured data (Table 1), 24 June corresponds to the lowest daily energy consumption, whereas 15 April exhibits the highest.

Table 3 also shows that, in the case of the symmetric inverter, the total phase line imbalance energy $\overline{E_{IMB}}$ does not depend on storage capacity and remains constant across all capacities, equal to the mean imbalance energy of 11 days given in Table 1 for the household grid without EES.

To clarify the origin of the parameter nonlinearity observed in the graphs shown in Figures 4–6, the power flow profiles over the course of two contrasting days were analyzed in detail. The days selected, 15 April and 6 June, were chosen due to their markedly different generation and consumption conditions, in order to illustrate how these differences affect the local power distribution between grid phase lines. On 15 April, the lowest generation among all days and comparatively high consumption were observed, whereas on 6 June, the opposite situation occurred, with the highest generation but rather moderate consumption.

Figure 7a,b show the daily imported energy E_{IMP} (dashed blue line) and exported energy E_{EXP} (dashed red line) for the inverter operating in symmetric mode, as well

as the corresponding energies E'_{IMP} and E'_{EXP} (solid lines) for the inverter operating in asymmetric mode, for 15 April (Figure 7a) and 6 June (Figure 7b). The absolute values of imported and exported energy in the asymmetric inverter mode are consistently lower than those in the symmetric inverter mode. It is also important to note that, as the storage capacity EC increases, the slope of the import and export characteristics is steeper in the asymmetric inverter case than in the symmetric inverter case. On 15 April, after applying the EES, energy import was reduced at maximum by 3534 Wh (21%) and energy export by 5543 Wh (40%) in the symmetric inverter mode. In contrast, under asymmetric inverter operation, energy import decreased by 7965 Wh (60%) and export by 9994 Wh (100%). On 6 June, in the symmetric inverter mode, energy import decreased by 269 Wh (8%) and export by 6747 Wh (9%), whereas in the asymmetric inverter mode, the corresponding reductions were 1700 Wh (71%) and 8193 Wh (12%), respectively. This demonstrates that the asymmetric inverter enables more effective utilization of EES in the household grid.

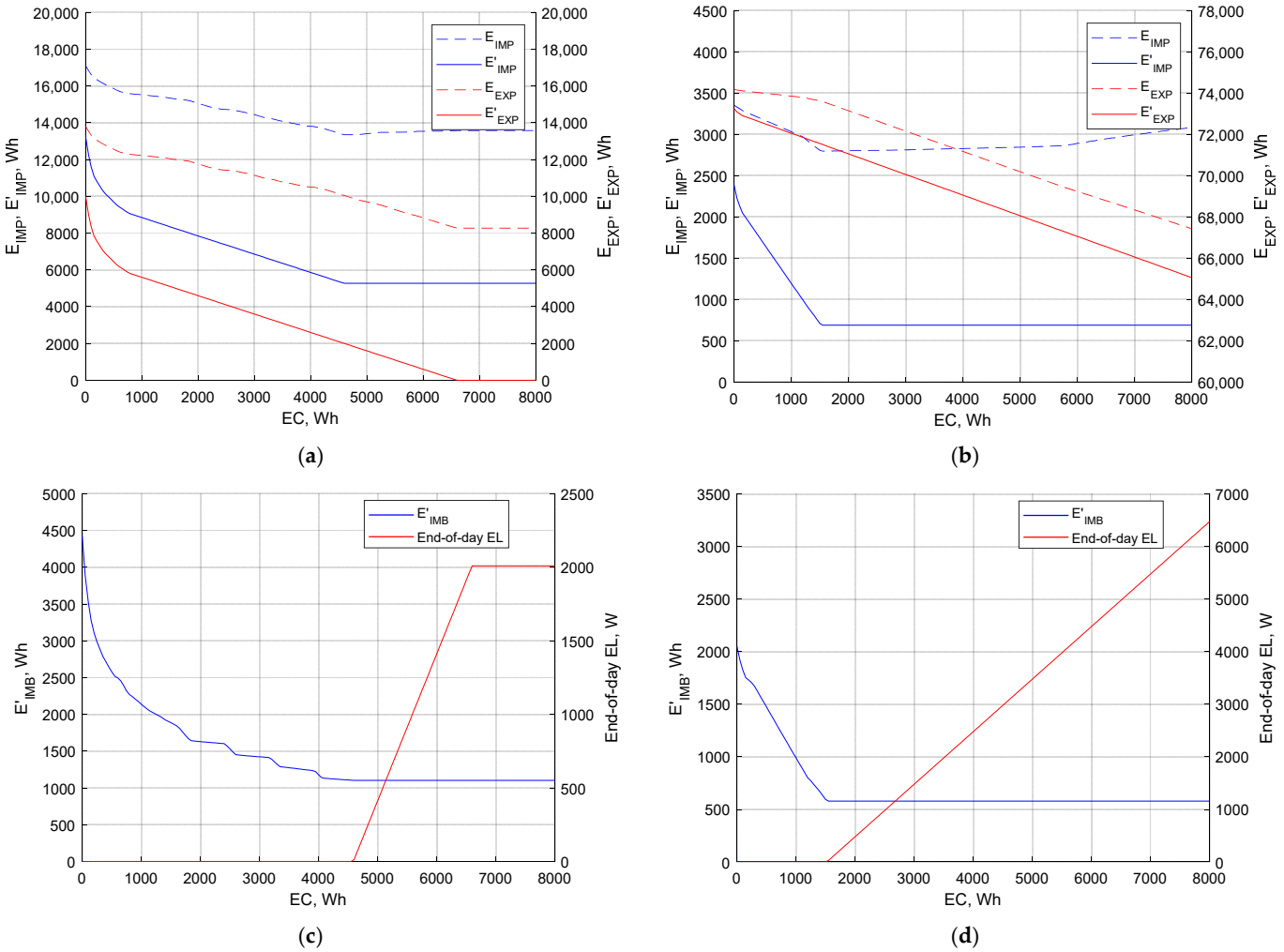

Figure 7. Dependencies of exported energies E_{EXP} and E'_{EXP}, imported energies E_{IMP} and E'_{IMP} (**a**,**b**), imbalance energy E'_{IMB}, and end-of-day EES energy level EL (**c**,**d**) on storage capacity for 15 April (**a**,**c**) and 6 June (**b**,**d**).

The primary factor determining the breakpoints in the dependencies of energy flows on storage capacity is the EES energy level at the end of the day (Figure 7c,d), which indicates the amount of stored but unused energy carried over to the next day. As long as the EES fully discharges by the end of the day, increasing storage capacity leads to a reduction in all energy flows. However, once a threshold capacity is reached, at which

the battery can no longer fully discharge (this occurs at approximately $EC = 4500$ Wh 15 March and at $EC = 1500$ Wh on 6 June), a breakpoint occurs, and energy import as well as total imbalance energy cease to decrease.

Further increases in capacity result in a growing amount of residual stored energy. As observed in the 15 March end-of-day EL profile (Figure 7c), another threshold is eventually reached at which the amount of stored energy ceases to increase. This is because all generated PV energy is either locally consumed or stored. At this stage, a breakpoint appears in the export curve, beyond which energy export no longer decreases.

4.3. Analysis of Parameters SSR and SCR in Symmetric and Asymmetric Inverter Modes

As mentioned earlier, the overall daily efficiency of energy distribution in the household grid was evaluated using the SCR and SSR parameters. These parameters were calculated for all eleven selected days for both the symmetric inverter case (SCR and SSR) and asymmetric inverter case (SCR' and SSR').

Figure 8 presents the dependencies of the parameters SCR (47) and SSR (46) on storage capacity for the symmetric inverter mode. In the proposed grid model, varying the storage capacity EC does not affect the locally consumed energy E_{CONS} and only affects the imported energy E_{IMP}. Consequently, the value of SSR, which depends on imported energy, increases with increasing storage capacity, and breakpoint is reached at the same capacity value at which the reduction in imported energy stabilizes (see Figure 4b).

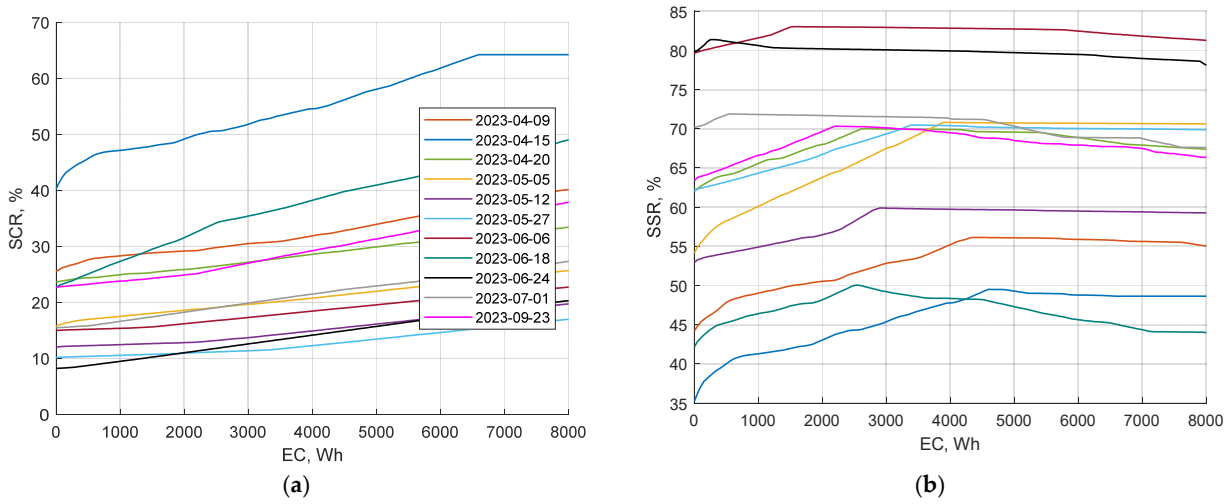

(**a**) (**b**)

Figure 8. Dependence of parameters SCR (**a**) and SSR (**b**) on storage capacity in symmetric inverter mode simulation.

The similar relation between the parameter SCR (Figure 8a) and exported energy E_{EXP} (Figure 4a) is observed. Since the generated energy E_{PV} (4) does not depend on the storage capacity, the entire change in parameter SCR is associated with variations in the exported energies. It increases with increasing storage capacity and stabilizes at the same breakpoint storage capacity value as in the export case (stabilization appears only on 15 April).

Figure 9 shows the obtained dependencies of the parameters SCR' and SSR' on EES capacitance EC for the asymmetric inverter operating mode. Both parameters reached higher values compared to the symmetric inverter mode. A rapid increase in their values is observed at relatively small storage capacities, which then slows until the breakpoint capacity is reached, beyond which the parameters remain constant (due to insufficient storage capacity, the breakpoint of the SCR' parameter is reached only on 15 April). Higher values of the parameter SCR' are obtained on days when solar generation is low compared

to the consumed power. Conversely, the parameter SSR' is higher when solar generation is high and a larger portion of the consumption demand is covered by it.

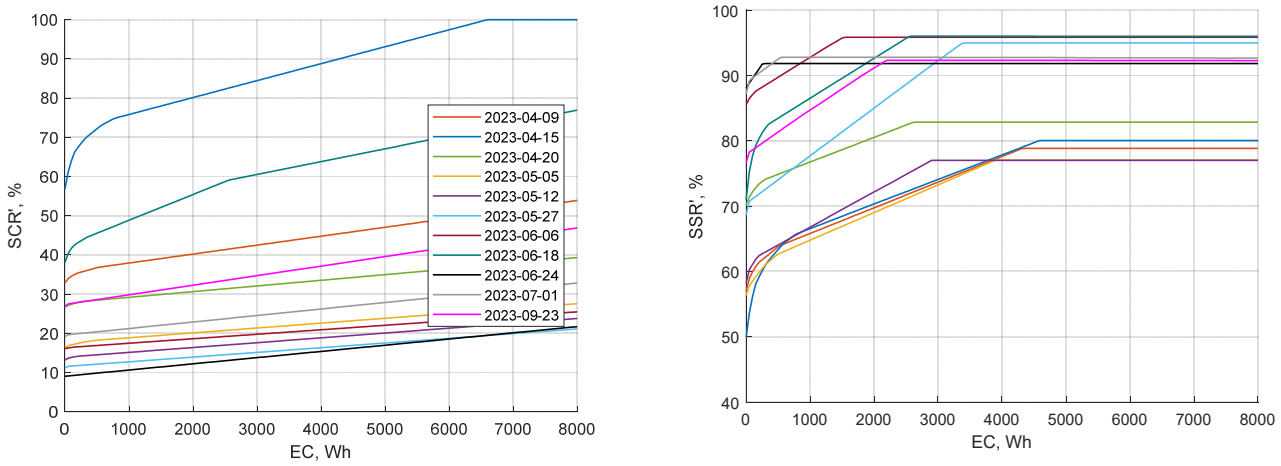

(**a**) (**b**)

Figure 9. Dependence of parameters SCR' (**a**) and SSR' (**b**) on storage capacity in asymmetric inverter mode simulation.

Since these efficiency parameters increase most rapidly at relatively small storage capacities and saturate at higher capacities, it is worth examining this small-capacity effect in more detail. Table 4 presents a difference between the SCR' parameter (asymmetric inverter case) and SCR parameter (symmetric inverter case) for the eleven investigated days at different storage capacities. Here, the storage capacity was increased in discrete 1000 Wh steps. The bottom row of the table presents the average difference $\overline{SCR' - SCR}$ between the two parameters for all analyzed days at the specified storage capacities.

Table 4. Difference between parameters SCR' and SCR at different storage capacities EC.

Day	***EC*, Wh**								
	0	**1000**	**2000**	**3000**	**4000**	**5000**	**6000**	**7000**	**8000**
	$SCR' - SCR$, %								
9 April 2023	7.3	9.6	11.0	11.9	12.9	13.1	13.2	13.4	13.7
15 April 2023	16.5	28.6	30.9	32.6	34.2	35.0	35.6	35.7	35.7
20 April 2023	3.0	4.2	4.7	4.9	4.9	5.0	5.3	5.7	5.9
5 May 2023	0.6	1.3	1.5	1.6	1.8	1.8	1.8	1.8	1.8
12 May 2023	1.1	2.6	3.5	3.9	3.9	3.9	3.9	4.0	4.0
27 May 2023	1.0	2.1	3.0	3.7	4.0	4.1	4.1	4.1	4.1
6 June 2023	1.1	2.1	2.4	2.4	2.4	2.4	2.5	2.6	2.7
18 June 2023	15.3	21.5	23.8	25.1	25.5	26.1	27.0	27.7	27.9
24 June 2023	0.8	1.1	1.2	1.2	1.2	1.2	1.2	1.3	1.4
1 July 2023	3.7	4.6	4.6	4.6	4.7	4.9	5.2	5.2	5.5
23 September 2023	4.2	6.0	7.3	7.6	7.9	8.2	8.4	8.6	9.0
	$\overline{SCR' - SCR}$, %								
	5.0	7.6	8.5	9.1	9.4	9.6	9.8	10.0	10.1

As can be seen from the results presented in the table, the asymmetric inverter operating mode is superior to the symmetric mode in terms of the self-consumption rate in all cases. As observed from the previous dependencies, increasing the energy storage capacity improves both the SCR and SCR' parameters; however, the improvement is more pronounced in the case of the asymmetric inverter. Under conditions of low solar generation, for example, on 15 April, increasing the storage capacity from 0 to 1 kWh increases the difference between SCR' and SCR by 73%. Under conditions of high solar generation, for example, on 6 June, the increase is even more pronounced: the difference between SCR' and SCR increases by 91%. On average, across all investigated days, the difference between SCR' and SCR increases by 42%, when a 1 kWh EES is applied.

As the storage capacity continues to increase, the growth in the difference between these parameters gradually diminishes and ultimately approaches a stable value. For instance, increasing the storage capacity from 7 kWh to 8 kWh results in an average increase of only about 1%. In this case study, the application of the EES resulted in more than a twofold increase in the difference between the SCR' and SCR' parameters, indicating the growing advantage of the asymmetric inverter. This shows that the storage system effectively enhances the advantages of the asymmetric inverter control algorithm for energy flow management.

Analogously to the analyzed parameters, Table 5 presents the difference between the SSR' parameter (asymmetric inverter case) and SSR parameter (symmetric inverter case) for the same eleven investigated days and average difference $\overline{SSR' - SSR}$ at the aforementioned storage capacities. The data presented here indicate that the asymmetric inverter operating mode is superior to the symmetric mode in all cases with respect to the self-sufficiency rate parameter. As shown, increasing the storage capacity from 0 to 1 kWh results in an average 51% increase in the difference between SSR' and SSR. However, the same increase in storage capacity from 7 kWh to 8 kWh increased the difference between these parameters by only 2%.

Table 5. Difference between parameters SSR' and SSR at different storage capacities EC.

Day	EC, Wh								
	0	**1000**	**2000**	**3000**	**4000**	**5000**	**6000**	**7000**	**8000**
	$SSR' - SSR$, %								
9 April 2023	12.8	16.8	19.2	20.8	22.4	22.8	23.0	23.2	23.8
15 April 2023	14.6	25.2	27.3	28.7	30.0	30.8	31.2	31.4	31.4
20 April 2023	8.0	11.2	12.5	12.9	13.0	13.3	14.0	15.0	15.5
5 May 2023	2.2	4.7	5.2	5.7	6.2	6.3	6.4	6.4	6.4
12 May 2023	5.2	11.8	15.7	17.1	17.3	17.4	17.5	17.6	17.7
27 May 2023	6.6	13.3	18.3	22.9	24.6	24.8	24.9	25.0	25.1
6 June 2023	5.9	11.2	12.8	12.9	13.0	13.1	13.4	14.0	14.6
18 June 2023	28.8	40.1	44.4	46.8	47.6	48.7	50.4	51.6	52.0
24 June 2023	8.3	11.2	11.6	11.8	11.9	12.1	12.3	12.9	13.7
1 July 2023	17.0	20.9	21.1	21.2	21.5	22.4	23.8	23.9	25.1
23 September 2023	13.2	18.1	21.5	22.2	22.8	23.8	24.4	24.8	25.9
	$\overline{SSR' - SSR}$, %								
	11.1	16.8	19.0	20.3	20.9	21.4	21.9	22.3	22.8

This indicates that, with respect to the SSR parameter, the relative efficiency at smaller storage capacities is higher than at larger capacities and that the impact of increasing storage capacity on efficiency decreases as the capacity grows. Overall, the use of the storage system increased the difference between the SCR' and SCR parameters by up to 22.8%. This also proves the enhanced efficiency of the storage system when combined with the asymmetric inverter algorithm.

The simulation shows that low-capacity energy storage systems (1–2 kWh) have the greatest impact on increasing the SCR and SSR parameters. As the energy storage capacity is further increased to 5–8 kWh, its influence on the growth of the SCR and SSR parameters becomes smaller compared to the effect of low-capacity energy storage systems. These results also demonstrate that intelligent control and optimal sizing are more important for sustainable energy systems than maximizing storage capacity.

4.4. Storage Capacity Impact on Daily Exported and Imported Power Flows

The previously presented simulation of dependencies of total daily energy import and export on storage capacity do not reveal the factors determining the breakpoint capacity level for a specific day, beyond which these quantities no longer decrease. This can only be clarified through a detailed second-by-second analysis of the daily power flow distribution. To investigate the variation in energy import, export, and phase line load asymmetry over the course of the day, a comprehensive analysis of daily power flows was conducted for all studied days. A more detailed analysis is presented using the examples of 15 April and 6 June, discussed earlier in Section 4.2.

Figure 10a shows the impact of energy storage capacity on the total exported power across the three phase lines P_{exp} (35) on 15 April. The time axis (x-axis) has a resolution of one second, and the sidebar color scale indicates the power magnitude in watts for each level. Similarly, Figure 10b presents the total imported power P_{imp} (34) for each second of the day at different storage capacities. These graphs present results obtained only for the symmetric inverter case.

The graphs illustrate at which times of day and how rapidly the import and export powers decrease as the storage capacity EC is increased. To facilitate the comparison of these power profiles at different storage capacities, four cross-sections of these graphs at storage capacities of 0, 1, 2, and 5 kWh are shown below (Figure 10c), depicting both the imported and exported power. For visual clarity, imported and exported power are depicted in blue and red with negative and positive values, respectively. Here, the power at zero storage capacity (cross-section $EC0$) corresponds to the import and export power measured during the experiment in the household without an EES system. This representation clearly demonstrates that, in the symmetric inverter mode, both energy import and export may occur simultaneously during periods of PV generation.

As the storage capacity increases, the export and import power profiles decrease; however, the rate of decrease is not uniform and varies over the course of the day. On 15 April, when solar generation is relatively low (see Table 1), the export power decreases until the storage capacity reaches approximately 6500 Wh. With further increases in capacity, export remains practically unchanged. In contrast, import decreases noticeably up to a capacity of approximately 4500 Wh and, as can be seen from the graph, remains unchanged in the morning, while the main change occurs in the evening. This is related to the fact that each simulation day starts with an empty storage system and, until solar generation begins in the morning, household grid import does not depend on storage capacity. As the storage capacity increases, a larger share of the energy accumulated during the day remains available to meet evening consumption, and as shown in Figure 10b, once a capacity of approximately 4500 Wh is reached, evening consumption is largely supplied from the

storage system and decreases only marginally thereafter, because the storage does not discharge completely until 24:00. This storage capacity represents a threshold beyond which further increases in capacity become only marginally effective in reducing energy import and export flows. Note that the specific numerical power values are characteristic only of this particular day under a specific solar generation and consumption scenario. Nevertheless, similar trends were observed on other days as well.

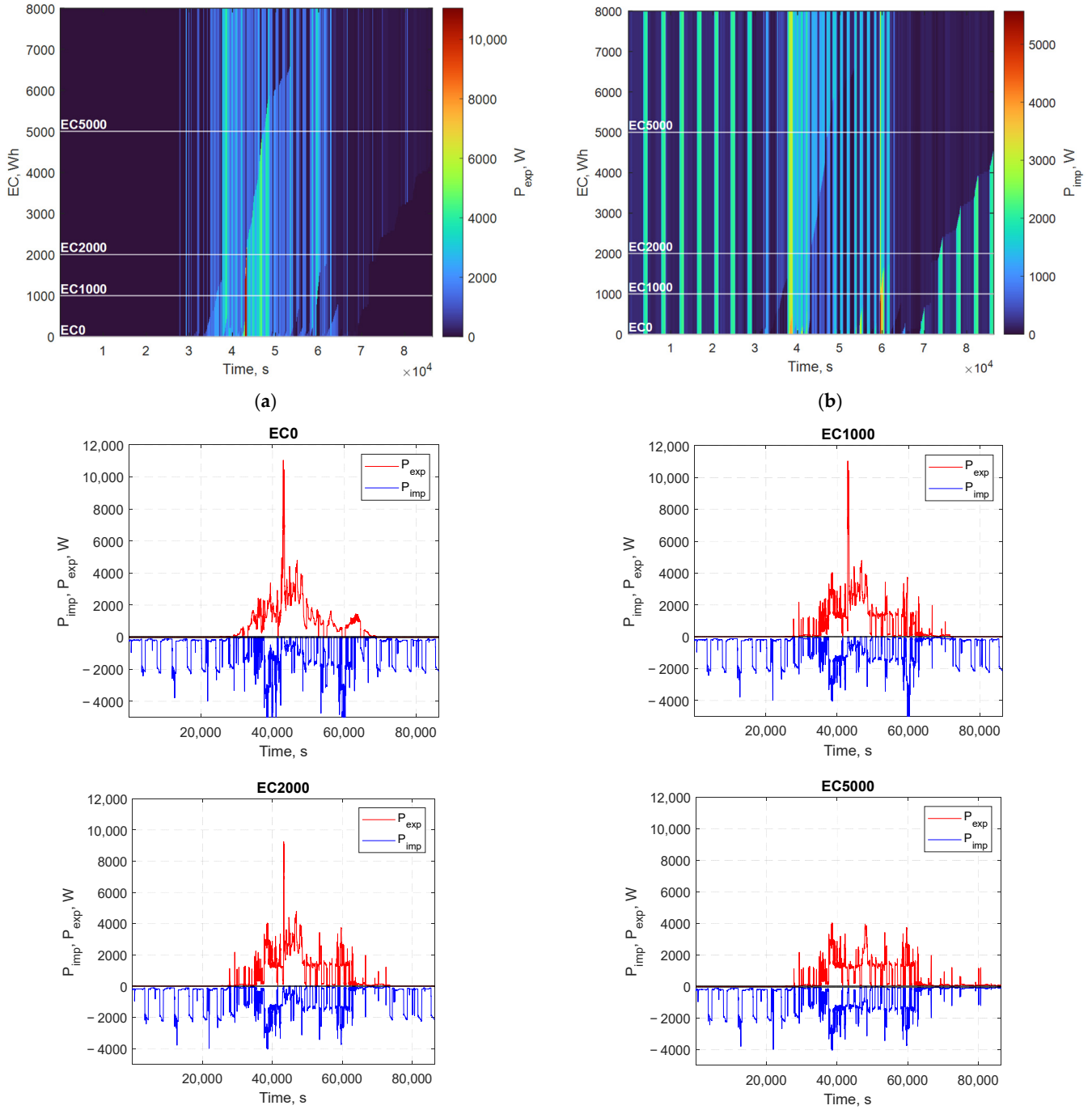

Figure 10. Influence of energy storage capacity EC on daily profiles of exported power P_{exp} (**a**) and imported power P_{imp} (**b**), and four particular cases of this dependance (**c**) in the case of the symmetric inverter on 15 April.

Figure 11 presents the daily power variation profiles for 6 June obtained for the symmetric inverter case. Unlike the 15 April example, on this day, the total solar generation was several times higher, while consumption was lower (Table 1). As a result, power export (Figure 11a) is significantly higher and, although it decreases as the storage capacity is increased, the threshold at which export reduction completely stabilizes is not reached. This indicates that the maximum storage capacity of 8000 Wh used in the model is insufficient to accumulate all the solar energy generated.

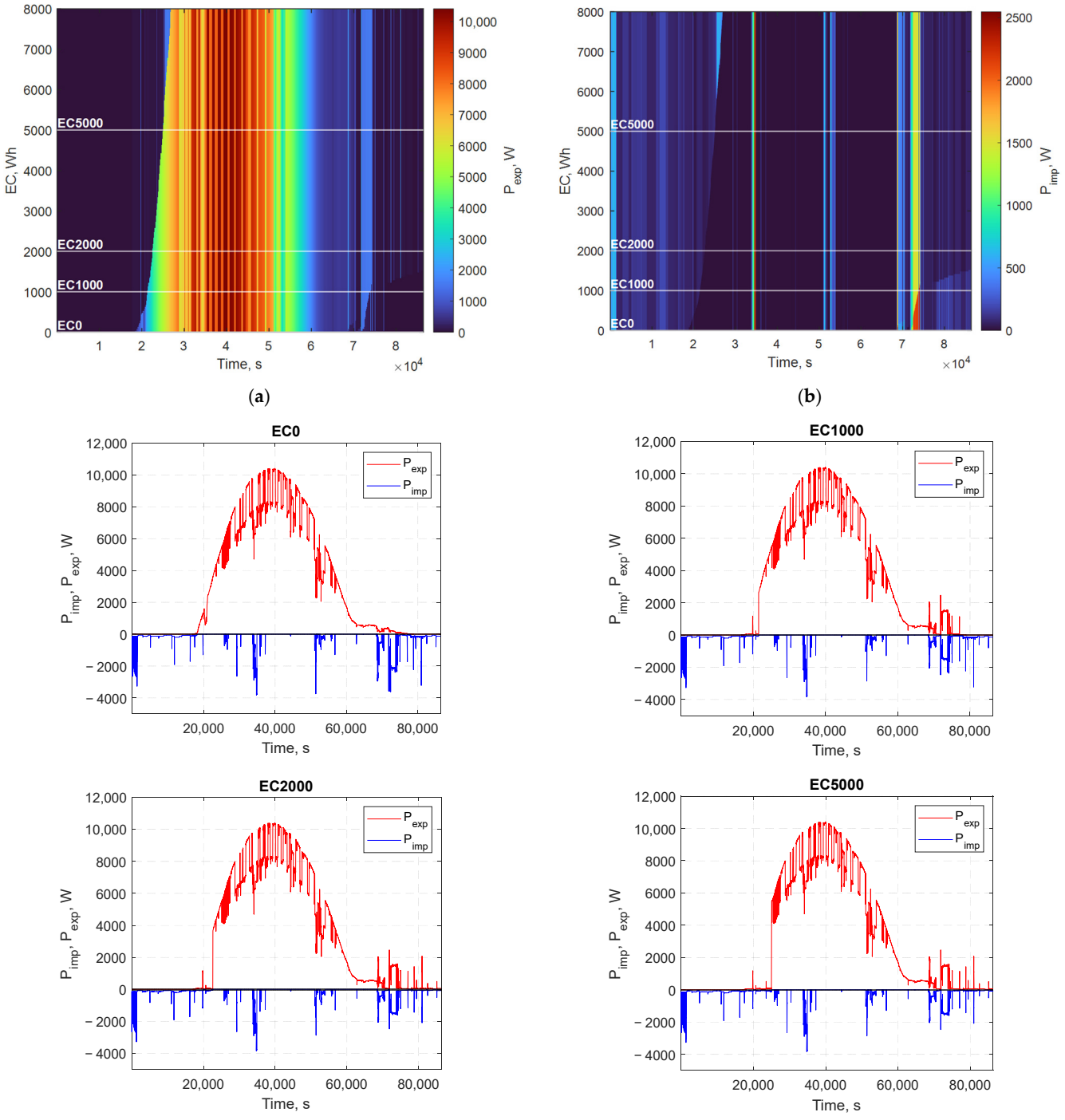

Figure 11. Influence of energy storage capacity EC on daily profiles of exported power P_{exp} (**a**) and imported power P_{imp} (**b**), and four particular cases of this dependance (**c**) in the case of the symmetric inverter on 6 June.

From the detailed import and export power profiles shown in Figure 11c, it can be observed that, when the storage system is connected, export decreases in the morning; however, in the evening, an additional exported power flow appears, which, in the absence of storage, was consumed locally.

As a result, the overall absolute change in export with increasing storage capacity is smaller than that on 15 April. Figure 11b shows that increasing the storage capacity also reduces import, and this reduction occurs mainly during the evening consumption period. At the same time, a slight increase in import is observed in the morning, which is related to the fact that, while the storage is charging, the grid inverter receives only the amount of energy required to satisfy the total three-phase consumption E_{CONS} (5) (see the storage control algorithm).

In turn, the symmetric grid inverter distributes the received energy equally among all three phases, and due to phase load imbalance, this energy is insufficient for the most heavily loaded phases, resulting in import, while the least loaded phases have excess energy, which is exported.

This effect is most pronounced when generation is low and the storage is not fully charged. Indeed, due to load asymmetry, energy export and import can occur simultaneously at any time of the day whenever solar generation is present and household consumption is taking place. This is illustrated in both Figures 10c and 11c.

Figures 12 and 13 present the corresponding graphs for the same days (15 April and 6 June, respectively), obtained for the asymmetric inverter mode. In this case, simultaneous bidirectional energy flows between the household grid and DSO grid are eliminated. This can be observed in the graphs shown in Figures 12c and 13c, where, as in the previous case, the daily import P_imp and export P_exp power profiles are shown for four different storage capacities.

For both days, significantly reduced import power levels are observed compared with the symmetric inverter case. This reduction, in absolute terms, increases with increasing storage capacity. At a certain storage capacity, evening import disappears in both cases, as the entire consumption demand is supplied from the EES system. Export in the asymmetric inverter case is also reduced, although to a lesser extent. Export is reduced most noticeably during the morning generation period, when the storage system is only beginning to charge. The influence of the storage system on export is more pronounced under conditions of lower daily solar generation.

As shown in Figure 12a, once a certain storage capacity (approximately 6500 Wh) is reached, export ceases because all surplus generated energy is accumulated in the storage system. In the case of the asymmetric inverter, the limiting storage capacities beyond which further increases in capacity become impractical are more clearly observed, as further capacity increases have only a minor effect on reducing energy import or export.

4.5. Storage Capacity Impact on Daily Imbalance Power

Figure 14 shows the influence of storage capacity *EC* on power imbalance P'_{imb} (39) in the household grid phase lines on 15 April. The daily imbalance profile is characterized by short peaks associated with abrupt changes in consumption, which can be effectively compensated with small-capacity EES through the injection of stored PV energy into the household grid. This is clearly illustrated by the four imbalance daily profiles corresponding to different storage capacities presented in Figure 14b.

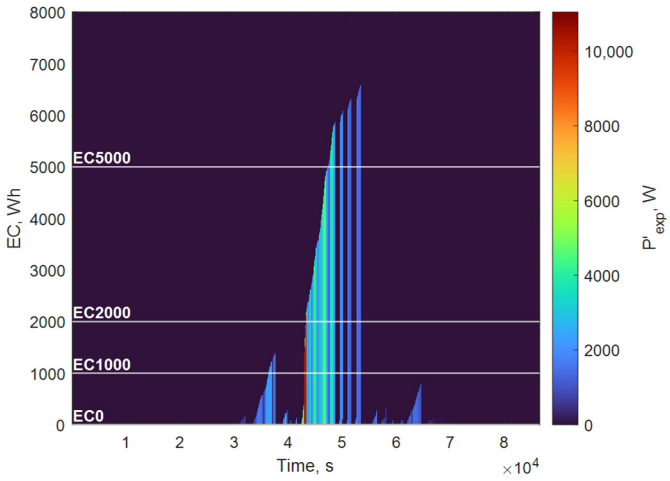

(**a**)

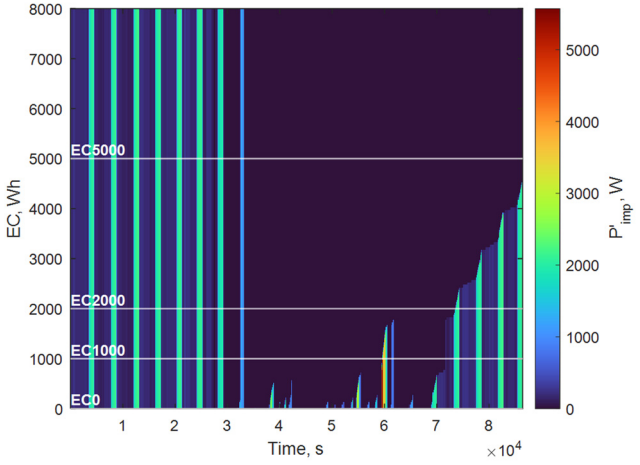

(**b**)

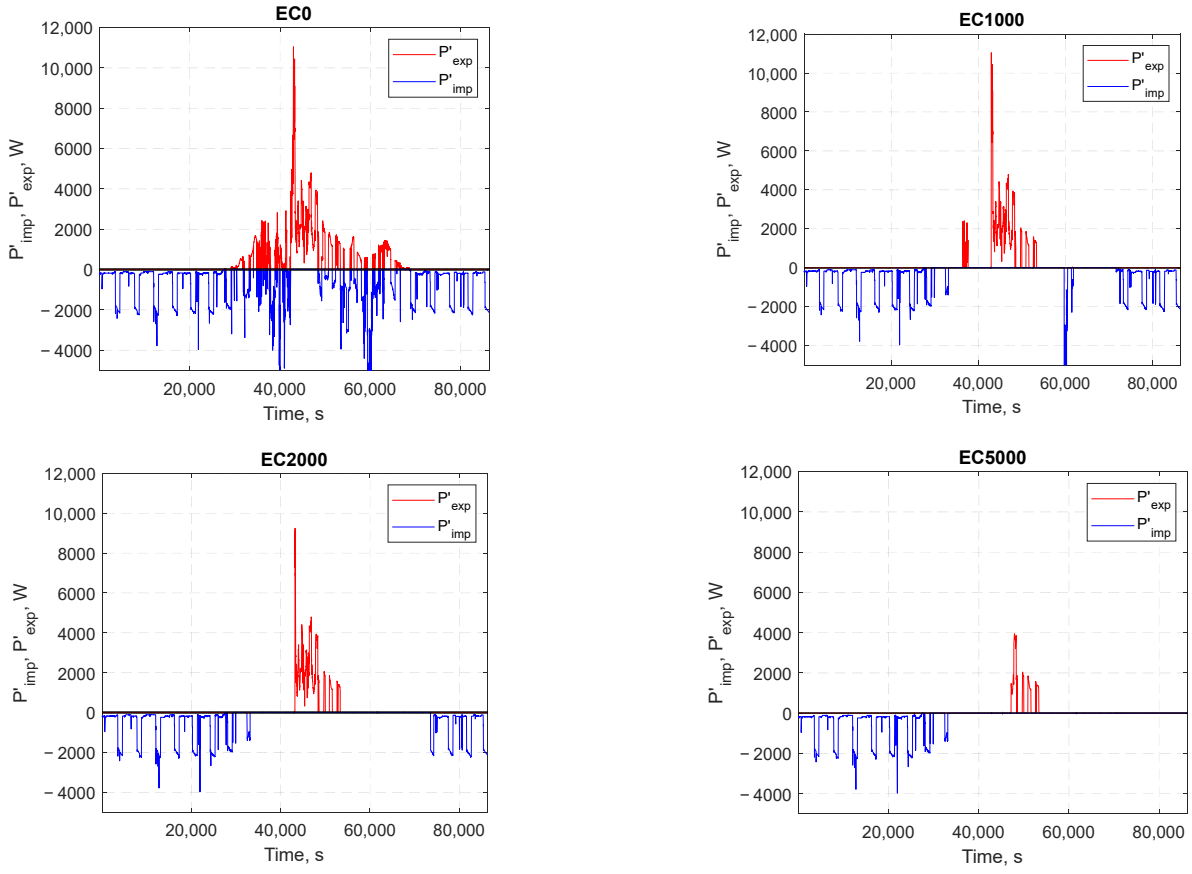

(**c**)

Figure 12. Influence of energy storage capacity EC on daily profiles of exported power P'_{exp} (**a**) and imported power P'_{imp} (**b**), and four particular cases of this dependance (**c**) in the case of the asymmetric inverter on 15 April.

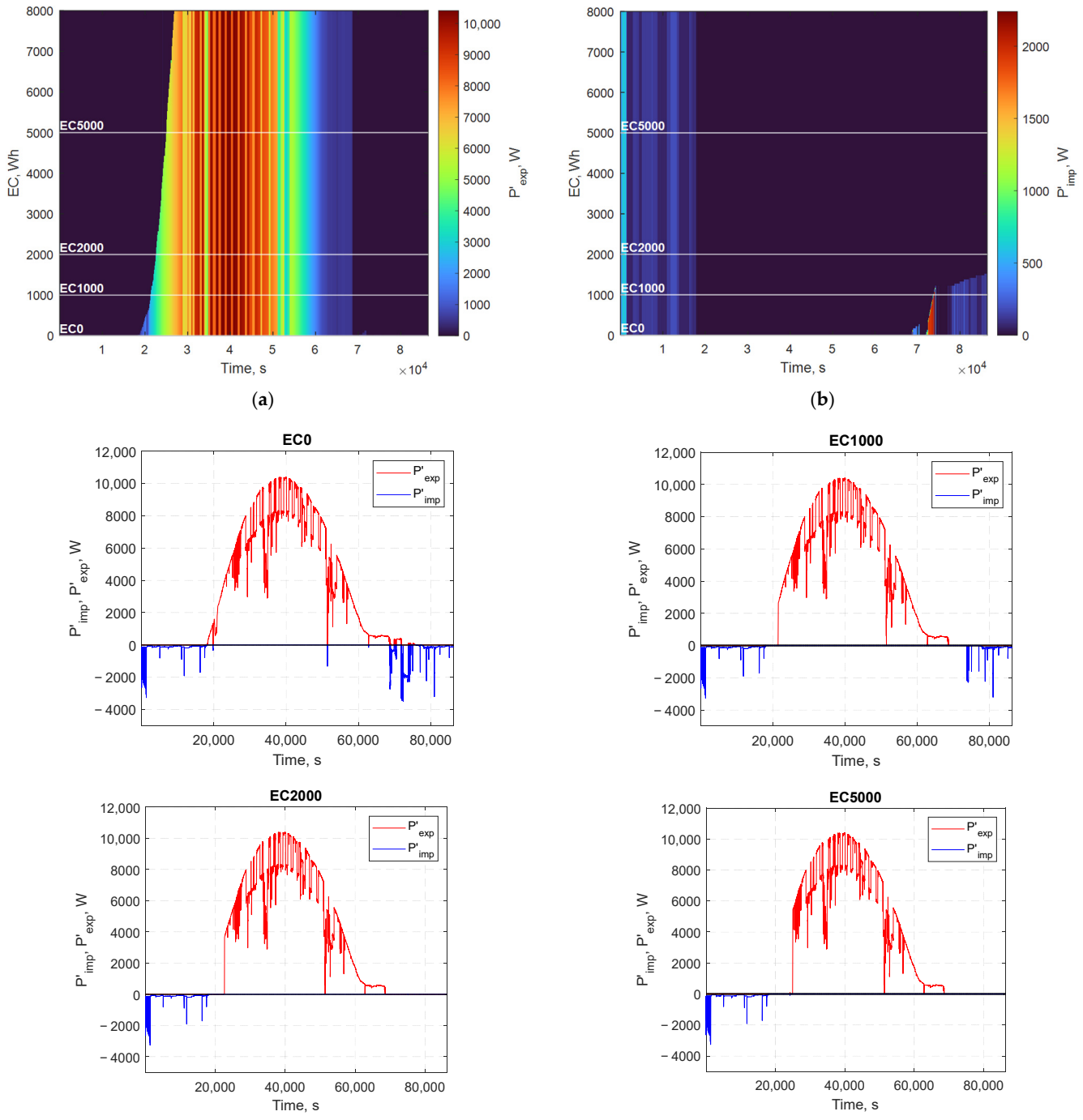

Figure 13. Influence of energy storage capacity EC on daily profiles of exported power P'_{exp} (**a**) and imported power P'_{imp} (**b**), and four particular cases of this dependance (**c**) in the case of the asymmetric inverter on 6 June.

With increasing storage capacity, the imbalance first disappears around midday and subsequently in the evening (see Figure 14a).

During the early hours of the day, however, the power flow imbalance is not affected by storage capacity. Therefore, the remaining daily imbalance energy E'_{IMB} (Figure 6) is primarily determined by the imbalance occurring at the beginning of the day and cannot be eliminated within the framework of the proposed model.

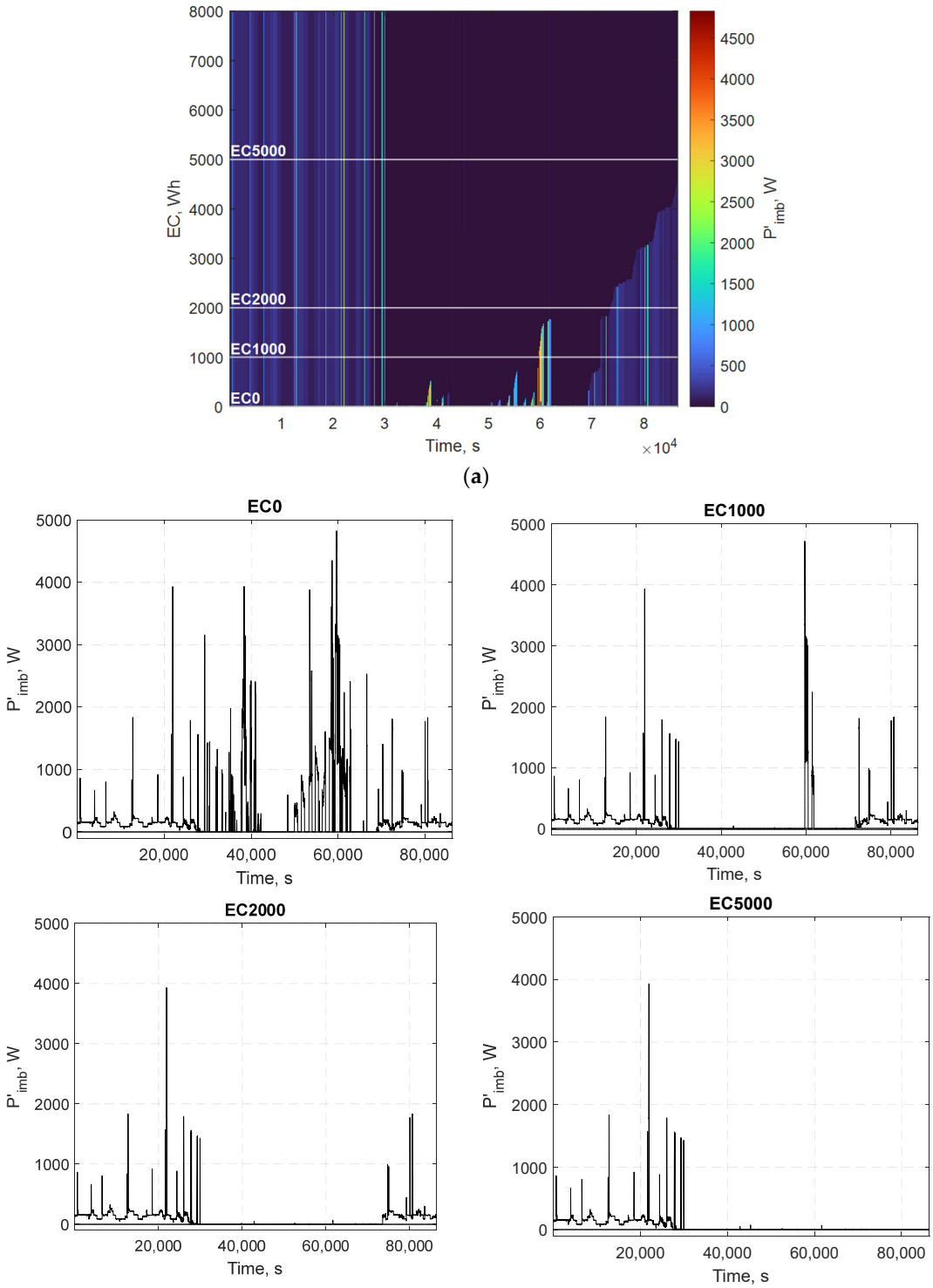

Figure 14. Influence of energy storage capacity EC on daily imbalance power P'_{imb} (**a**), and four particular cases of this dependance corresponding to different storage capacities (**b**) on 15 April.

Figure 15 illustrates the dependence of power imbalance P'_{imb} on storage capacity EC at different times of the day on 6 June. Due to higher PV generation, a larger share of the generated energy is used to satisfy local consumption and to symmetrize phase line power flows. Consequently, a smaller storage capacity is sufficient to achieve the minimum daily imbalance energy, as only a relatively small imbalance emerging in the evening needs to be compensated.

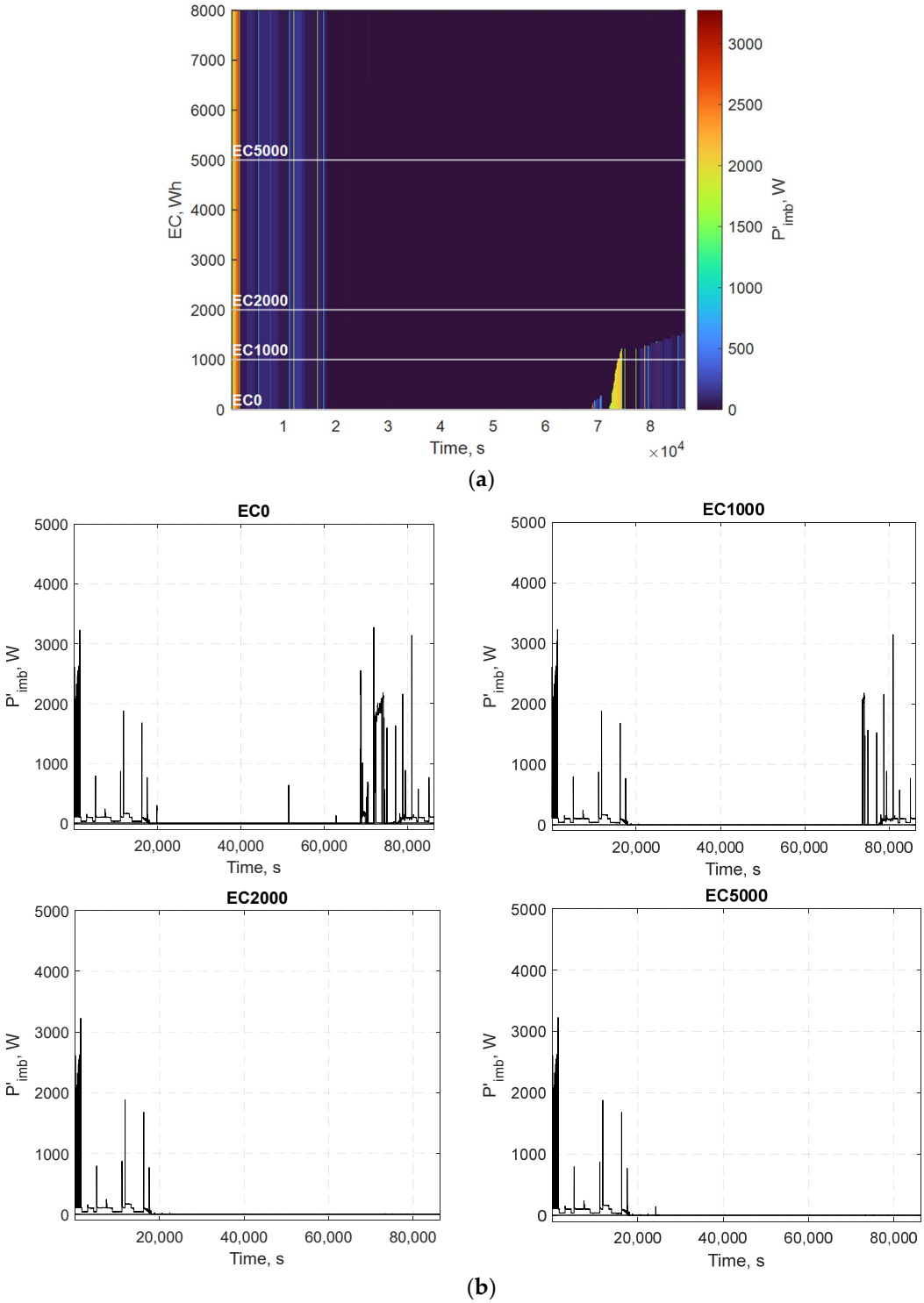

Figure 15. Influence of energy storage capacity *EC* on daily imbalance power P'_{imb} (**a**), and four particular cases of this dependance corresponding to different storage capacities (**b**) on 6 June.

The presented examples illustrate the seasonal variation in energy flows in the prosumer grid. The results indicate that under conditions of higher PV generation (on 6 June), the energy required for consumption and balancing is supplied directly through PV generation. Consequently, a smaller energy storage capacity *EC* (2 kWh) is sufficient to meet consumption demand and ensure balancing. In this case, only a minor evening imbalance needs to be compensated. Under conditions of lower PV generation (on 15 April), a larger energy storage capacity *EC* (5 kWh) is required to satisfy consumption demand and ensure balancing.

With detailed, complete one-year data on household generation and consumption, it would be possible to propose an efficient forecasting-based strategy for the utilization of available storage resources across all four seasons. In this manner, the reduced seasonal storage demand would free up resources that could be used, for example, for trading on the electricity market. This could also serve as a basis for further research.

5. Discussion

The main objective of this study was to validate the proposed simulation methodology and identify key trends in the interactions between energy storage systems, inverter control, and household energy flows. The simulation results are based on real data from a single household. For this purpose, a typical household with a 10 kWp photovoltaic system was selected, and representative days from the spring, summer, and autumn periods were analyzed. During this period, the ratio of daily PV energy generation to energy consumption varied from 0.87 (15 April) to 9.72 (24 July).

The proposed system operates efficiently when the energy generated by the PV panels is sufficient to both balance energy exchange across the phase lines of the DSO grid and charge the energy storage system, which can subsequently be used for balancing in the absence of generation. In regions with lower solar irradiance, higher-capacity PV systems would be required, whereas in regions with higher solar availability, smaller systems may be sufficient. The winter period was not included in this study, as PV generation in Lithuania is negligible due to limited solar irradiance and frequent snow coverage. It should also be noted that the proposed methodology can be extended to other types of household generation systems, such as small-scale wind power plants.

According to the National Electrical Manufacturers Association (NEMA), the phase imbalance factor is intended for assessing unidirectional power flow imbalance in phase lines and is not suitable for cases involving bidirectional power flows. In this study, due to PV generation and asymmetric household consumption, bidirectional power flows frequently occur across the phase lines (i.e., generation in one phase and consumption in another). Under such conditions, the conventional imbalance factor may yield misleading average values. To address this, imbalance is evaluated using the maximum signed difference between phase line power flows, defined as imbalance power P_{imb} and imbalance energy E_{IMB}. For similar reasons, the evaluation of neutral current is not considered informative in this context.

Simulations were carried out using measured household grid power values, i.e., the values after a specific symmetric inverter; therefore, system losses were inherently included. However, when simulating both symmetric and asymmetric inverter operation with different EES capacities, the components were assumed to be ideal. Consequently, the measured output power of the symmetric inverter P_{inv} without EES was considered equal to the PV generated power P_{pv}. This assumption was adopted to evaluate the theoretical potential for improving PV energy utilization and reducing energy exchange with the DSO grid.

The use of an idealized EES model in this study is intended for conceptual analysis. In practice, EES technologies exhibit diverse characteristics and operational constraints. Here, an idealized representation was employed to simplify the modeling framework, which is sufficient for assessing the fundamental behavior of the proposed approach. The system performance is determined by the PV generation power P_{pv} and the household phase line load powers P_{consLi} at each time step. The PV generated power is used both for redistribution among the household phase lines and for charging the EES system.

In the case of a symmetric inverter, the generated PV power is distributed equally among all three household phase lines P_{consLi}, regardless of their individual loads. Any

surplus energy is stored in the EES and later supplied back to the household grid when PV generation becomes insufficient or unavailable. As a result, both daily electricity export E_{EXP} and import E_{IMP} are reduced. With an EES capacity of 8 kWh, the average energy import $\overline{E_{IMP}}$ across the analyzed days decreases by 16%, while the export $\overline{E_{EXP}}$ decreases by 13%. However, the daily imbalance energy E_{IMB} remains unaffected, since the differences in simultaneous import and export power flows P_{dsoLi} across the phase lines do not change.

In contrast, when an asymmetric inverter operates according to the APFM algorithm, the PV generation power is first redistributed among the phase lines P'_{consLi} based on their instantaneous loads. This reduces the differences between phase line powers P'_{dsoLi} and improves the symmetry of the DSO grid load. Any remaining excess PV power is used to charge the EES system. When PV generation is insufficient or absent, the stored energy is supplied back to the household grid and redistributed in the same manner, i.e., according to the phase line loads. As a result, daily energy import E'_{IMP}, export E'_{EXP}, and imbalance energy E'_{IMB} are further reduced. For an EES capacity of 8 kWh, the average energy import $\overline{E'_{IMP}}$ decreases by 56%, energy export $\overline{E'_{EXP}}$ by 19%, and imbalance energy $\overline{E'_{IMB}}$ by up to 75% across the analyzed days. Note that these results represent an idealized scenario and may be less pronounced when using real energy storage systems. In practice, the achievable benefits will depend on system specific parameters, particularly the efficiency of energy storage and retrieval. The impact of these parameters will be investigated in future work.

Residual stored energy at the end of the day primarily occurs at relatively large storage capacities. However, the results indicate that the most significant benefits of EES are achieved at smaller capacities. Therefore, future work will focus on addressing an optimization problem aimed at achieving the best system performance with minimal storage capacity. Under such conditions, inter-day energy carry-over is expected to be relatively limited. Nevertheless, any carry-over of stored energy to the following day is expected to further improve grid performance parameters and overall energy utilization efficiency.

6. Conclusions

This study analyzes the impact of an EES system on power flows in a prosumer's three-phase household grid under two different inverter operating modes: a conventional symmetric mode and an adaptive asymmetric mode based on the Adaptive Power Flow Management algorithm. The entire analysis is based on the simulation of household power flows using real measured data of energy import, export, consumption, and PV generation from a specific residential installation. Once the primary data were obtained, simulation was performed using a 1 s time resolution.

A comparative analysis of phase power imbalance parameters obtained using different time resolutions (1 s, 15 min, and 1 h) revealed that higher resolution enables more accurate detection of rapid short-term imbalance variations, which are averaged out at lower resolutions. For example, increasing the resolution from 1 h to 1 s results in an average 2.8 times increase in maximum phase imbalance and 1.5 times increase in its daily standard deviation. This significantly affects the accuracy of derived parameters such as the total daily imbalance energy, self-sufficiency rate, and self-consumption rate.

The simulation results show that combining EES with an asymmetric inverter significantly reduces phase imbalance and energy exchange with the DSO grid. Most improvements occur at relatively small EES capacities (1–2 kWh), with diminishing gains at higher capacities. Over the analyzed period, the EES operating with the asymmetric inverter reduced the total household imbalance energy E'_{IMB} by an average of 72%. This parameter strongly correlates with energy consumption and import: higher daily imports result in

higher imbalance, and vice versa. Moreover, the EES paired with a symmetric inverter does not reduce this imbalance energy and has no effect on it.

The simulation results also show that, across all analyzed days, the application of an 8 kWh EES enabled an average reduction in energy import of 16% in symmetric mode and 56% in asymmetric mode, while energy export decreased by 13% and 19%, respectively. These results indicate that the asymmetric inverter operating mode improves EES utilization compared with the symmetric mode, resulting in increased prosumer autonomy and enhanced household grid performance.

The impact of EES capacity on household energy distribution efficiency was evaluated using SCR and SSR. Without EES, SCR in the asymmetric case is 5% higher than in the symmetric case; with an 8 kWh EES, this difference increases to 10.1%. A similar trend is observed for SSR: 11.1% without EES and 22.8% with EES. The largest performance gains occur at low capacities: increasing EES capacity from 0 to 1 kWh improves SCR by approximately 42% and SSR by about 51%, whereas increasing capacity from 7 to 8 kWh yields only an additional 1–2% improvement.

Overall, the results demonstrate that combining an adaptive asymmetric inverter control algorithm with an appropriately sized energy storage system enables more efficient utilization of on-site PV energy while simultaneously improving the load symmetry of the phase lines in the DSO grid. This study contributes to the development of smart energy flow management strategies aimed at enhancing the efficiency of prosumer household-integrated energy systems and reducing hardware resource requirements.

Author Contributions: Conceptualization, L.Š., M.V., A.B. and S.G.; methodology, L.Š., M.V., A.B. and G.S.; software, L.Š., J.D. and G.V.; validation, L.Š. and A.B.; formal analysis, L.Š., M.V. and A.B.; investigation, L.Š. and J.D.; resources, A.B.; data curation, L.Š., M.V., A.B. and G.S.; writing—original draft preparation, L.Š., M.V. and A.B.; writing—review and editing, L.Š., M.V., A.B., and G.S.; visualization, L.Š. and J.D.; supervision, M.V., A.B. and G.S.; project administration, S.G.; funding acquisition, S.G. All authors have read and agreed to the published version of the manuscript.

Funding: This research was funded by the Research Council of Lithuania (LMTLT) and the Ministry of Education, Science and Sport of the Republic of Lithuania, agreement No: S-A-UEI-23-1, and by the Economic Revitalization and Resilience Enhancement Plan "New Generation Lithuania", agreement No. 02-002-P-0001.

Data Availability Statement: The data presented in this study are available on request from the corresponding author due to restrictions related to the privacy of private household owners.

Conflicts of Interest: The authors declare no conflicts of interest.

Abbreviations

The following abbreviations are used in this manuscript:

APFM	Adaptive Power Flow Management
PV	Photovoltaic
DSO	Distribution System Operator
SSR	Self-Sufficiency Rate
SCR	Self-Consumption Rate
EES	Electric Energy Storage
EC	Energy Capacity

References

1. Climate Change. Energy and Climate are Inextricably Linked. Available online: https://www.iea.org/topics/climate-change (accessed on 14 February 2026).
2. Chen, Q.; Kuang, Z.; Liu, X.; Zhang, T. Transforming a solar-rich county to an electricity producer: Solutions to the mismatch between demand and generation. *J. Clean. Prod.* **2022**, *336*, 130418. [CrossRef]
3. Jiang, Q.; Khattak, S.I.; Rahman, Z.U. Measuring the simultaneous effects of electricity consumption and production on carbon dioxide emissions (CO_2e) in China: New evidence from an EKC-based assessment. *Energy* **2021**, *229*, 120616. [CrossRef]
4. Mishra, S.; Saini, G.; Saha, S.; Chauhan, A.; Kumar, A.; Maity, S. A survey on multi-criterion decision parameters, integration layout, storage technologies, sizing methodologies and control strategies for integrated renewable energy system. *Sustain. Energy Technol. Assess.* **2022**, *52*, 102246. [CrossRef]
5. Lu, Z.; Wang, J.; Shahidehpour, M.; Bai, L.; Li, Z.; Yan, L.; Chen, X. Risk-Aware Flexible Resource Utilization in an Unbalanced Three-Phase Distribution Network Using SDP-Based Distributionally Robust Optimal Power Flow. *IEEE Trans. Smart Grid* **2024**, *15*, 2553–2569. [CrossRef]
6. Šriupša, L.; Vaitkūnas, M.; Baronas, A.; Dosinas, J. Analysis of Self-Generated PV Energy Consumption Profiles in Prosumers Microgrid. *Int. J. Sustain. Energy* **2023**, *42*, 1583–1602. [CrossRef]
7. Huangfu, C.; Wang, E.; Yi, T.; Qin, L. Low-Voltage Distribution Network Loss-Reduction Method Based on Load-Timing Characteristics and Adjustment Capabilities. *Energies* **2024**, *17*, 1115. [CrossRef]
8. Naveen Babu, M.; Dhal, P.K. Impact of load flow and network reconfiguration for unbalanced distribution systems. *Meas. Sens.* **2024**, *32*, 101078. [CrossRef]
9. Khan, A.; Ali, M. Three-Phase Load Balancing in Distribution Systems Using Load Sharing Technique. *Eng. Proc.* **2023**, *46*, 18. [CrossRef]
10. Chang, C.-K.; Cheng, S.-T.; Boyanapalli, B.-K. Three-Phase Unbalance Improvement for Distribution Systems Based on the Particle Swarm Current Injection Algorithm. *Energies* **2022**, *15*, 3460. [CrossRef]
11. Rus-Casas, C.; Gilabert-Torres, C.; Fernández-Carrasco, J.I. Optimizing Energy Management and Sizing of Photovoltaic Batteries for a Household in Granada, Spain: A Novel Approach Considering Time Resolution. *Batteries* **2024**, *10*, 358. [CrossRef]
12. Hassan, Q.; Pawela, B.; Hasan, A.; Jaszczur, M. Optimization of Large-Scale Battery Storage Capacity in Conjunction with Photovoltaic Systems for Maximum Self-Sustainability. *Energies* **2022**, *15*, 3845. [CrossRef]
13. Osorio, F.; Mantilla, M.A.; Rey, J.M.; Petit, J.F. A Flexible Control Strategy for Multi-Functional PV Inverters with Load Compensation Capabilities Considering Current Limitations and Unbalanced Load Conditions. *Energies* **2024**, *17*, 4218. [CrossRef]
14. Eyimaya, S.E.; Altin, N.; Nasiri, A. Optimization of Photovoltaic and Battery Storage Sizing in a DC Microgrid Using LSTM Networks Based on Load Forecasting. *Energies* **2025**, *18*, 3676. [CrossRef]
15. Jakus, D.; Novaković, J.; Vasilj, J.; Jolevski, D. Optimal Residential Battery Storage Sizing Under ToU Tariffs and Dynamic Electricity Pricing. *Energies* **2025**, *18*, 2391. [CrossRef]
16. Rezaeimozafar, M.; Barrett, E.; Monaghan, R.F.D.; Duffy, M. Optimal sizing of behind-the-meter battery energy storage systems under optimal battery operation: A case study in Ireland. *J. Energy Storage* **2024**, *87*, 111324. [CrossRef]
17. Ciocia, A.; Amato, A.; Di Leo, P.; Fichera, S.; Malgaroli, G.; Spertino, F.; Tzanova, S. Self-Consumption and Self-Sufficiency in Photovoltaic Systems: Effect of Grid Limitation and Storage Installation. *Energies* **2021**, *14*, 1591. [CrossRef]
18. Rinio, M. Economic Benefit of a Photovoltaic System and Impact of a Battery Using Real Data from a Swedish House. *Energies* **2025**, *18*, 5658. [CrossRef]
19. Vahabi Khah, M.; Zahedi, R.; Eskandarpanah, R.; Mirzaei, A.M.; Noudeh Farahani, O.; Malek, I.; Rezaei, N. Optimal sizing of residential photovoltaic and battery system connected to the power grid based on the cost of energy and peak load. *Heliyon* **2023**, *9*, e14414. [CrossRef]
20. Pinthurat, W.; Hredzak, B. Distributed Control Strategy of Single-Phase Battery Systems for Compensation of Unbalanced Active Powers in a Three-Phase Four-Wire Microgrid. *Energies* **2021**, *14*, 8287. [CrossRef]
21. Held, L.; Mueller, F.; Steinle, S.; Barakat, M.; Suriyah, M.R.; Leibfried, T. An Optimal Power Flow Algorithm for the Simulation of Energy Storage Systems in Unbalanced Three-Phase Distribution Grids. *Energies* **2021**, *14*, 1623. [CrossRef]
22. Li, S.; Zhang, T.; Liu, X.; Liu, X. A Battery Capacity Configuration Method of a Photovoltaic and Battery System Applied in a Building Complex for Increased Self-Sufficiency and Self-Consumption. *Energies* **2023**, *16*, 2190. [CrossRef]
23. Kesküla, A.; Grjaznov, K.; Sepp, T.; Allik, A. Optimal Sizing of Residential PV and Battery Systems Under Grid Export Constraints: An Estonian Case Study. *Energies* **2025**, *18*, 4405. [CrossRef]
24. Rezaeimozafar, M.; Monaghan, R.F.D.; Barrett, E.; Duffy, M. A review of behind-the-meter energy storage systems in smart grids. *Renew. Sustain. Energy Rev.* **2022**, *164*, 112573. [CrossRef]
25. Markotić, T.; Šljivac, D.; Marić, P.; Žnidarec, M. Sustainable Integration of Prosumers' Battery Energy Storage Systems' Optimal Operation with Reduction in Grid Losses. *Sustainability* **2025**, *17*, 7165. [CrossRef]

26. Osman, M.G.; Lazaroiu, G.; Hamad, S.A.; Messaoud, H.; Mohammed, D.; Stoica, D. Analysis of Photovoltaic Systems with Battery Storage, Electric Vehicle Charging, and Smart Energy Management. *Sustainability* **2025**, *17*, 3887. [CrossRef]
27. Tu, R.; Guo, Z.; Liu, L.; Wang, S.; Yang, X. Reviews of Photovoltaic and Energy Storage Systems in Buildings for Sustainable Power Generation and Utilization from Perspectives of System Integration and Optimization. *Energies* **2025**, *18*, 2683. [CrossRef]
28. Van Someren, C.; Visser, M.; Slootweg, H. Sizing Batteries for Power Flow Management in Distribution Grids: A Method to Compare Battery Capacities for Different Siting Configurations and Variable Power Flow Simultaneity. *Energies* **2023**, *16*, 7639. [CrossRef]
29. Carpinelli, G.; Noce, C.; Russo, A.; Varilone, P.; Verde, P. Optimal siting and sizing of battery energy storage systems in unbalanced distribution systems: A multi-objective problem under uncertainty. *Int. J. Electr. Power Energy Syst.* **2024**, *162*, 110316. [CrossRef]
30. Šriupša, L.; Vaitkūnas, M.; Baronas, A.; Svinkūnas, G.; Dosinas, J.; Knyš, A.; Gudžius, S.; Jonaitis, A.; Serva, D. Enhancing the Efficiency of Photovoltaic Power Flows Management in Three-Phase Prosumer Grids. *Sustainability* **2025**, *17*, 2134. [CrossRef]